



Vietnamese-German University

COPYRIGHT WARNING

This paper is protected by copyright. You are advised to print or download **ONE COPY** of this paper for your own private reference, study and research purposes. You are prohibited having acts infringing upon copyright as stipulated in Laws and Regulations of Intellectual Property, including, but not limited to, appropriating, impersonating, publishing, distributing, modifying, altering, mutilating, distorting, reproducing, duplicating, displaying, communicating, disseminating, making derivative work, commercializing and converting to other forms the paper and/or any part of the paper. The acts could be done in actual life and/or via communication networks and by digital means without permission of copyright holders.

The users shall acknowledge and strictly respect to the copyright. The recitation must be reasonable and properly. If the users do not agree to all of these terms, do not use this paper. The users shall be responsible for legal issues if they make any copyright infringements. Failure to comply with this warning may expose you to:

- Disciplinary action by the Vietnamese-German University.
- Legal action for copyright infringement.
- Heavy legal penalties and consequences shall be applied by the competent authorities.

The Vietnamese-German University and the authors reserve all their intellectual property rights.



Bachelor Thesis

Thermodynamic assessment of high-temperature heat pump concepts for industrial applications

Submitted by: Tran Cong Luan

RUB student ID: 19219993

VGU student ID: 14502



First examiner: Prof. Dr.-Ing Roland Span

Second examiner: Dr.-Ing Monika Thol

Supervisor: Dr.-Ing Stefan Glos

November 2022

Lehrstuhl für Thermodynamik

Fakultät für Maschinenbau



THERMODYNAMIK

Thermodynamic assessment of high-temperature heat pump concepts for industrial applications

A Thesis Presented

By

Tran Cong Luan

Submitted to the department of Mechanical Engineering of the

**RUHR-UNIVERSITÄT BOCHUM and VIETNAMESE-GERMAN
UNIVERSITY**



Of the requirement for the degree of

BACHELOR IN MECHANICAL ENGINEERING

November 2022

Major: Mechanical Engineering

Affirmation in lieu of oath

Tran, Cong Luan

Matriculation Number: 19219993

Title of Thesis: Thermodynamic assessment of high-temperature heat pump concepts for industrial applications

I hereby declare in lieu of oath that I have produced the aforementioned thesis independently and without using any other means except the aids listed. Any thoughts directly or indirectly taken from somebody else's sources are made discernible as such. To date, the thesis has not been submitted to any other board of examiners in the same or a similar format and has not been published yet.

Bochum, 10.11.2022



Tran Cong Luan



Vietnamese-German University

Blocking note

The presented bachelor thesis with the title "Thermodynamic evaluation of high-temperature heat pump concepts for industrial applications" contains internal confidential data of Siemens Energy Global GmbH & Co. KG. It is only to be made accessible to the first and second reviewers and, if applicable, to the chairperson of the examination board of the Department of Mechanical Engineering. Publications and duplications of the bachelor thesis, or the passing on of the bachelor thesis - in whole or in part as well as the making of copies or transcripts - also in digital form - are generally prohibited. Exceptions require the prior written approval of Siemens Energy Global GmbH & Co. KG."



Vietnamese-German University

Acknowledgement

I would like to express my thanks to the following people for helping me greatly with my thesis and for making my stay in Germany during this time highly enjoyable.

Special thanks to my supervisor Dr. Stefan Glos. Although the process of composing the thesis was not always smooth, his patience, encouragements, and thoughtful remarks had shown me many new insights and more importantly, the aspects that I could still improve on. It would have been great if I were better at having conversations, but I thoroughly enjoyed our small chats.

I would also like to thank the Chair of Thermodynamics and the Mechanical Engineering Student Council of Ruhr Universität Bochum for organizing such an awesome trip to Germany.

I would like to express my deepest gratitude to my friends, who had embarked with me on this journey halfway across the globe (well 9000 km was not halfway but it was still pretty far). All the game nights, all the journeys to another cities or countries and all the times that I was dragged away from working just to have a bit of fun will be deeply missed. Thank you for the happiest four years of my life, for revising with me knowledge from the courses that we were so happy that we had survived and for putting up with my moans about the thesis, although I did complete it quite early.

Finally, I dedicate the last line to my family, without whom I would not have met all these wonderful people and make these memories. Their unconditional support will always be a motivation for me to push through life, even in times when I doubt myself the most.

Abstract

Waste heat recovery is one of the approaches that still has great potential in achieving the goal of global decarbonization. Thus, the aim of this bachelor thesis was to design and analyze a system that utilized waste heat provided by end-use processes to produce steam and power, which would then be fed back into the chemical sites.

The modules that would be used for this system were the industrial heat pump and SHARC design, which was a newly developed system by Siemens Energy. The redesign and calculation process of these modules were done in Siemens internal program called KRAWAL. A constraint variation analysis was performed on the redesigned models. Then, comparisons were carried out to determine the most efficient variant for each module.

Finally, the complete design was created, which included two industrial heat pumps in combination of a SHARC system. This final system was compared to a previously investigated system and showed greater exergetic efficiency of 65.2% and lower power consumption of 1285 MW.



Vietnamese-German University

Table of Contents

Title Page	I
Affirmation in lieu of oath	II
Blocking note	III
Acknowledgement	IV
Abstract	V
Tables of Contents	VI
List of Figures	VIII
List of Tables	XII
Formula characters and symbols	XIII
1. Introduction	1
1.1. Motivation of Thesis	1
1.2. Thesis overview	4
2. Theoretical background	6
2.1. Heat pump principle.....	6
2.2. State of the art	8
3. Boundary conditions and requirements	11
4. Architectures of the investigated systems	13
4.1. Description of the investigated systems	13
4.2. Industrial Heat pump.....	13
4.2.1. Intercooling with spray water	17
4.2.2. Intercooling with heat storage	18
4.3. Direct steam evaporation design	19
4.4. SHARC design.....	19
4.4.1. Additional turbines design	20
4.4.2. Steam extraction from second and third expansion stages	22
4.4.3. Steam extraction from first and second expansion stages	24
5. Constraint variation analysis	27
5.1. Description of constraint variation analysis.....	27

5.2. Methodology	27
5.2.1. System performance	27
5.2.2. Data collection method	29
5.3. Constraint variation analysis of industrial heat pump.....	29
5.3.1. Steam evaporation pressure	29
5.3.2. Waste heat inlet temperature	34
5.3.3. Waste heat outlet temperature	40
5.4. Constraint variation analysis of SHARC design	44
5.4.1. Steam extracted mass flow	44
5.4.2. Waste heat temperature	47
6. Comparison analysis of different systems.....	49
6.1. Comparison analysis description.....	49
6.2. Industrial heat pump.....	49
6.2.1. Intercooling methods.....	49
6.2.2. Direct steam evaporation design	50
6.3. SHARC design.....	53
6.3.1. Performance comparison.....	53
6.3.2. Maximum amount of extractable steam	55
7. Final system	57
7.1. Overall architecture.....	57
7.2. CO ₂ heat pump with Carnot battery system	58
7.3. Performance comparison between two systems.....	58
8. Conclusion	61
9. Outlook.....	63
Bibliography	64

List of Figures

Figure 1.1.1.	Final energy consumption of various industrial sectors in EU28 (2016) [MSZ+ 21].....	1
Figure 1.1.2.	Simplified scheme of the supply structure of a typical modern chemical site [BPK+ 22].....	2
Figure 1.1.3.	Simplified block scheme of an iUI for chemical sites [BPK+ 22] ...	3
Figure 2.1.1.	Schematic of reverse Rankine cycle [HuAn 10] (Left) and T-s diagram of the reverse ideal Rankine cycle [McG 14] (Right).....	6
Figure 2.1.2.	Schematic of a reverse Brayton cycle [HuAn 10] (Left) and T-s diagram of a reverse Brayton cycle [WaZh 18] (Right).....	7
Figure 4.2.1.	Schematic of industrial heat pump (Heat-pump cycle numbered) .	13
Figure 4.2.2.	Schematic of industrial heat pump (Steam-compression module numbered).....	14
Figure 4.2.3.	Pressure-Volume diagram of different compression processes [NLN 19].....	15
Figure 4.2.4.	Pressure-Volume diagram of compression with intercooling [Cas 22].....	16
Figure 4.2.5.	T-s diagram of the heat pump cycle at baseline conditions.....	17
Figure 4.2.6.	Schematic diagram of industrial heat pump with spray water intercooling.....	18
Figure 4.2.7.	Schematic diagram of industrial heat pump with heat storage intercooling.....	18
Figure 4.3.1.	Schematic of direct steam evaporation design.....	19
Figure 4.4.1.	SHARC module with its Charging cycle (Left) and Generation cycle (Right)	19
Figure 4.4.2.	T-s diagram of SHARC's Generation cycle with single expansion line	21
Figure 4.4.3.	T-s diagram of SHARC's Generation cycle with double expansion lines.....	21
Figure 4.4.4.	T-s diagram of SHARC's Generation cycle at baseline (for steam extraction from 2 nd and 3 rd expansion stages).....	22
Figure 4.4.5.	T-s diagram of SHARC's Generation cycle at the adjustment limit (for steam extraction from 2 nd and 3 rd expansion stages)	23

Figure 4.4.6.	Schematic of SHARC's modified Generation cycle (for steam extraction from 2 nd and 3 rd expansion stages).....	24
Figure 4.4.7.	T-s diagram of SHARC's adjusted Generation cycle (for steam extraction from 1 st and 2 nd expansion stages).....	25
Figure 4.4.8.	Schematic of SHARC's modified Generation cycle (for steam extraction from 1 st and 2 nd expansion stages).....	26
Figure 5.3.1.	Schematic of industrial heat pump with indication of steam evaporation pressure	30
Figure 5.3.2.	Industrial heat pump's (whole system) COP (Left) and Exergetic efficiency (Right) with respect to the variation of steam evaporation pressure.....	31
Figure 5.3.3.	T-s diagrams of heat-pump cycle at steam evaporation pressure of 0.35 bars (Left) and 1.55 bars (Right)	33
Figure 5.3.4.	Industrial heat pump's volumetric flow of steam with respect to variation in steam evaporation pressure.....	34
Figure 5.3.5.	Theoretical COP of a heat pump with respect to heat source and sink temperature (Left) and T-s diagram of Carnot cycle (Right)..	35
Figure 5.3.6.	Industrial heat pump's (whole system) COP (Left) and Exergetic efficiency (Right) with respect to variation of waste heat inlet temperature	36
Figure 5.3.7.	COP of the heat-pump cycle in the industrial heat pump system with respect to waste heat inlet temperature.....	37
Figure 5.3.8.	T-s diagram of Carnot cycle under the effect of medium fluid's evaporation temperature variation	37
Figure 5.3.9.	T-s diagrams of heat-pump cycle for the waste heat inlet temperature of 30°C (Left) and 90°C (Right).....	38
Figure 5.3.10.	T- \dot{Q} diagrams of the heat-pump cycle's condenser for the waste heat inlet temperature of 30°C (Left) and 90°C (Right).....	38
Figure 5.3.11.	T- \dot{Q} diagrams of heat-pump cycle's evaporator for waste heat inlet temperature of 30°C (Left) and 90°C (Right).....	39
Figure 5.3.12.	Industrial heat pump's (whole system) COP (Left) and Exergetic efficiency (Right) with respect to the variation of steam evaporation pressure at waste heat inlet temperature of 90°C.....	40

Figure 5.3.13.	Industrial heat pump's (whole system) COP (Left) and Exergetic efficiency (Right) with respect to variation of waste heat outlet temperature	41
Figure 5.3.14.	T-s diagrams of the heat-pump cycle for waste heat outlet temperature of 20°C (Left) and 40°C (Right).....	41
Figure 5.3.15.	Mass flow of waste heat with respect to the variation of waste heat outlet temperature	42
Figure 5.3.16.	T- \dot{Q} diagrams of heat-pump cycle's evaporator for waste heat outlet temperature of 20°C (Left) and 40°C (Right).....	42
Figure 5.3.17.	Summary diagrams for industrial heat pump's COP (Left) and Exergetic efficiency (Right) with respect to variation of waste heat temperature levels.....	43
Figure 5.4.1.	SHARC module's exergetic efficiency with respect to variation of steam extraction mass flow (for extraction from 2 nd and 3 rd expansion stages).....	44
Figure 5.4.2.	Relative change of mass flows in SHARC module with respect to low-pressure steam extraction from second expansion stage	45
Figure 5.4.3.	T- \dot{Q} diagram of "Salt heat exchanger 4" in the Generation cycle...	46
Figure 5.4.4.	SHARC module's exergetic efficiency with respect to variation of steam extraction mass flow (for extraction from 1 st and 2 nd expansion stages).....	46
Figure 5.4.5.	Summary diagram of SHARC module's exergetic efficiency with respect to variation of waste heat temperature.....	47
Figure 5.4.6.	T-s diagram of SHARC's heat-pump cycle for waste heat inlet temperature of 30°C (Left) and 90°C (Right).....	47
Figure 5.4.7.	T-s diagram of SHARC's heat-pump cycle for waste heat outlet temperature of 20°C (Left) and 40°C (Right).....	48
Figure 6.2.1.	COP (Left) and Exergetic efficiency (Right) of variants of the industrial heat pump.....	49
Figure 6.2.2.	COP (Left) and Exergetic efficiency (Right) of direct steam evaporation design with respect to variation of steam evaporation pressure.....	50
Figure 6.2.3.	T- \dot{Q} diagram of evaporator at the upper pressure limit.....	51

Figure 6.2.4.	T- \dot{Q} diagram of evaporator at the lower pressure limit.....	52
Figure 6.2.5.	Volumetric flow of steam with respect to variation of steam evaporation pressure	53
Figure 6.3.1	Summary diagram of SHARC's exergetic efficiency with respect to the variation of extracted steam mass flow.....	54
Figure 6.3.2.	Summary diagram of required waste heat mass flow with respect to the variation of extracted steam mass flow.....	54
Figure 6.3.3.	Maximum amount of extractable medium-pressure steam for each variant of SHARC module.....	55
Figure 6.3.4.	T- \dot{Q} diagram of Oil heat exchanger in the Charging cycle.....	55
Figure 6.3.5.	Outlet temperature of the water flow through Oil heat exchanger in the Charging cycle with respect to variation of extracted steam mass flow	56
Figure 7.1.1.	Schematic of the final design and requirements for each module ..	57
Figure 7.2.1.	Schematic of the combined system of CO ₂ -based heat pump and Carnot battery	58



List of Tables

Table 1.	Requirements from the chemical sites	11
Table 2.	Boundary conditions of waste heat and feedwater	11
Table 3.	Power consumption and exergetic efficiency of the current and previous systems	59



Vietnamese-German University

Formula characters and symbols

Formula characters

COP	$[-]$	Coefficient of Performance
η_{ex}	$[-]$	Exergetic efficiency
P	$[MW]$	Power
\dot{Q}	$[MW]$	Heat flow
W	$[MJ]$	Work
Q	$[MJ]$	Heat
$q; dq$	$\left[\frac{J}{kg}\right]$	Specific heat / - infinitesimal difference
$w; dw$	$\left[\frac{J}{kg}\right]$	Specific work / - infinitesimal difference
V	$[m^3]$	Volume
\dot{V}	$\left[\frac{m^3}{s}\right]$	Volumetric flow
$p; \Delta p; dp$	$[bar]$	Pressure/ - difference / - infinitesimal difference
$T; \Delta T$	$[K]$	Temperature/ - difference
\dot{m}	$\left[\frac{kg}{s}\right]$	Mass flow
$\dot{E}; \Delta \dot{E}$	$[MW]$	Exergy flow/ - difference
$s; \Delta s; ds$	$\left[\frac{J}{kg \cdot K}\right]$	Entropy/ - difference/ - infinitesimal difference
$h; \Delta h$	$\left[\frac{kJ}{kg}\right]$	Specific enthalpy / - difference

Symbols

η	$[-]$	Efficiency
--------	-------	------------

Abbreviations

EU28	28 countries of the European Union
GHG	Greenhouse Gas
FEC	Final Energy Consumption
CHP	Combined Heat and Power

iUI	Ideal Utility Infrastructure
T-s	Temperature – Entropy
T- \dot{Q}	Temperature – Heat flow
p-V	Pressure – Volume
TES	Thermal Energy Storage
SHARC	Supercritical H ₂ O Application Rankine cycle
KRAWAL	Kraftwerksauslegung
VBA	Visual Basic for Application (from Excel)
HX	Heat Exchanger
CO ₂	Carbon Dioxide
H ₂ O	Water

Indices

<i>diss</i>	Dissipation
<i>rev</i>	Reversible
<i>ex</i>	Exergetic
<i>out / in</i>	Outlet / Inlet
<i>a</i>	Ambient
<i>Carnot</i>	Carnot cycle
<i>H / C</i>	Hot / Cold

1. Introduction

1.1. Motivation of Thesis

By 2050, the 28 countries of the European Union (EU28) aimed to cut down 80% of current greenhouse gas (GHG) as part of the transition to a future of low carbon society [KSM 20]. One of the most direct objectives of this agreement was the reduction of the final energy consumption (FEC) in energy intensive industries, especially in the industrial sector [MSZ+ 21].

The main approaches to achieve decarbonization include improvement of process efficiency, implementation of new processes, waste heat recovery and conversion from fossil energy and feedstock to renewable sources [MSZ+ 21]. The implementation and research of renewable energy in industrial processes were already quite popular [MSS 11], [KRD+ 16]. However, the potential of low-grade heat and the technology to recover it was reported to be still not fully exploited and hence, more attention should be given. Specifically, low-grade heat of under 200°C was still largely emitted to the ambient rather than recovered [HZB+ 16]. This source of waste heat could still be avoided by employing additional heat recovery system.

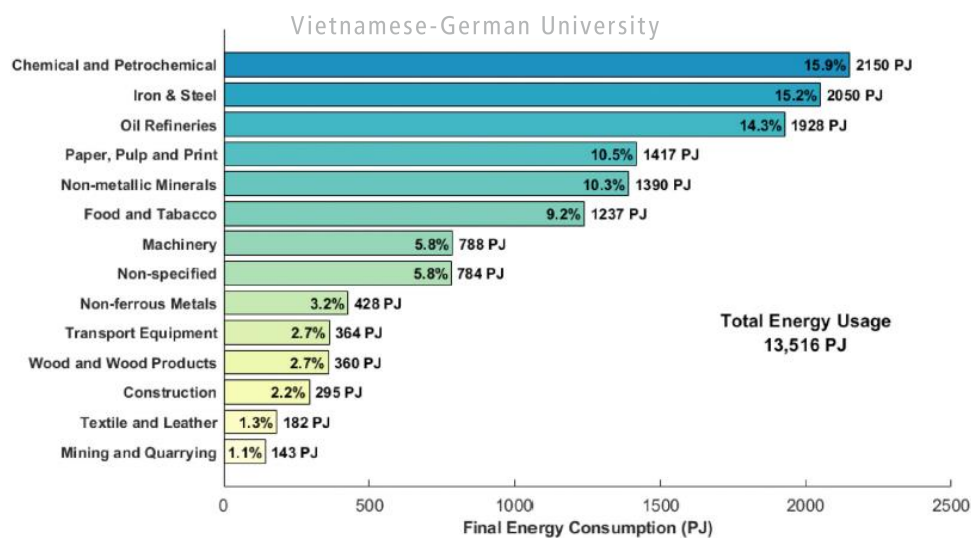


Figure 1.1.1. Final energy consumption of various industrial sectors in EU28 (2016) [MSZ+ 21]

Aside from that, the determination of the industrial sector that is most subjected to greenhouse gas reduction is also vital. Figure 1.1. shows the amount of final energy consumptions of different industrial sectors in EU28. Alongside with Iron & Steel industries and Oil Refineries, the sector of Chemical & Petrochemical accounted for the greatest proportion of consumed energy in 2016. Thus, this sector was one of the energy-intensive industries that had been targeted to reduce carbon dioxide emission [CAN 22].

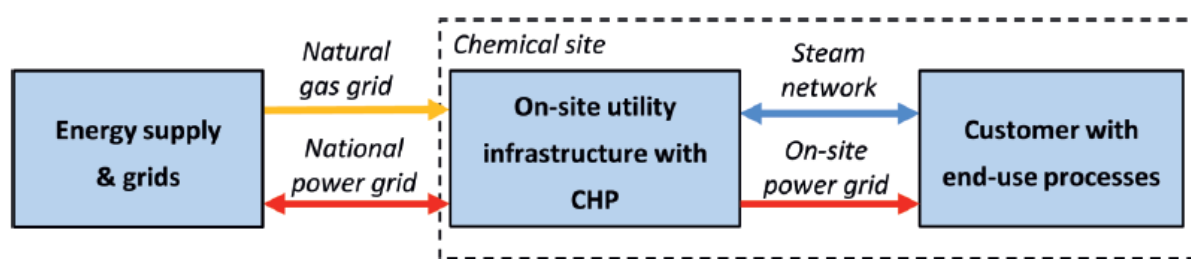


Figure 1.1.2. Simplified scheme of the supply structure of a typical modern chemical site [BPK+ 22]

A typical modern chemical site supply structure is shown in Figure 1.1.2. One of the compartments that determines the system performance is the utility infrastructure, which generates electricity and steam for the end-use demands by commonly utilizing a CHP unit (also known as cogeneration) [BPK+ 22]. The use of cogeneration instead of separate production, such as a power plant and a boiler, reduces the heat losses significantly due to the unit's high efficiency (commonly from 65% to 90%) [DiRo 20]. Thus, Chemical & Petrochemical sector has had a long history of CHP implementation [BPK+ 22].

Due to the maturity of the utility infrastructure technology, this paper focuses instead on the recovery potential of waste heat, which is intended to reduce the amount of consumed fossil fuel and power by the utility infrastructure. Low-grade heat, the by-product of chemical processes, is removed from the system through water or air coolers if no heat recovery system is used, which is a major source of energy loss [Kir 15]. One solution for this problem, and also the main topic of this paper, is the utilization of the heat pump concept. Heat pump has great benefits in terms of its low-grade heat utilization and CO₂ emission compared to direct fuel combustion processes. Despite that, The European market for heat pumps was considered to be still full of potential [PGZ 17]. For a market of heat pump up to 200°C, calculations showed that 641 PJ/year of power of process heat of the industrial sector in general and 283 PJ/year in the chemical sector specifically could be covered by heat pumps [MSZ+ 21]. Moreover, heat pump could be integrated with

existing technologies to further improve the system performance. For example, a cogeneration process with incorporated gas engine saw higher efficiency and yielded greater carbon savings. Also, renewable energy technologies could already combine with heat pumps to reduce basic fuel input [CCY 10].

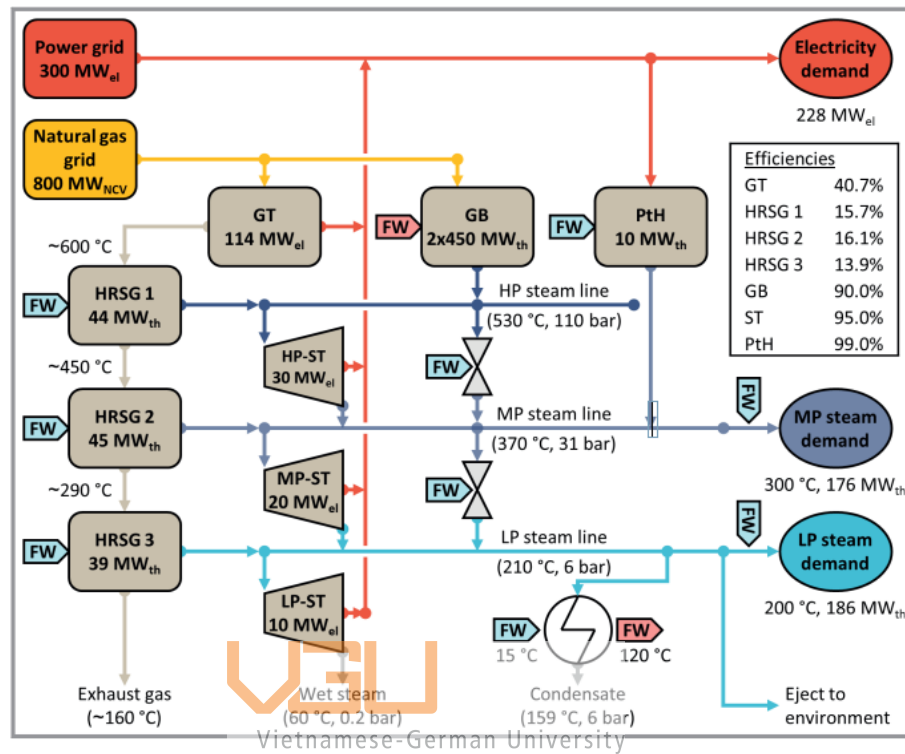


Figure 1.1.3. Simplified block scheme of an iUI for chemical sites [BPK+ 22]

The reference boundary conditions for this thesis were obtained from an already existing literature work, which is simplified as the schematic in figure 1.1.3. [BPK+ 22]. In this reference paper, an ideal Utility Infrastructure (iUI) had been developed based on steam and power demand from existing chemical sites in Germany. The purpose of the proposed heat recovery system is to minimize the amount of consumed power and natural gas through the generation of additional steam and power from otherwise rejected heat as a by-product of chemical sites activities. Therefore, the output requirements of the mentioned paper, specifically the temperature, pressure, and rate of heat flow values of the steam outputs were used for the proposed system.

In summary, this paper aims to contribute towards the global decarbonization by serving as a stepping stone for the popularization of high-temperature heat pumps in the industrial sector. The goal of this work is the complete thermodynamics analysis of heat pump

concepts for industrial applications. Then, the most optimal system shall be designed based on the boundary conditions from chemical sites. The generation of useful heat (steam) and electricity as the outputs of the system will be the focus of this paper. Further investigation could be carried out on cold generation in future studies.

1.2. Thesis overview

In the second chapter, the theoretical background for this thesis is given. This chapter gives a brief overview of the basic principles of heat pump and different thermodynamic cycles that conventional heat pumps operate on. The state-of-the-art technology and operational range of heat-pump systems are also discussed in this chapter.

The third chapter presents the demands from the chemical sites and the boundary conditions of the investigated system. Then, the variants of the system modules are described in the fourth chapter. The industrial heat pump and a newly developed Carnot battery system called SHARC were the modules of the complete system that had been investigated. The default models were provided by Siemens Energy and redesigned to match the demands.



Vietnamese-German University

Chapter five reports the procedure and results of the constraint variation analysis for both the industrial heat pump and the SHARC design. For the industrial heat pump, the varied constraints included the evaporation pressure of steam, the inlet and outlet temperature of the supplied waste heat. Meanwhile, the mass flow of extracted steam, the inlet and outlet temperature levels of waste heat were the modified in the SHARC design investigation.

The comparison of the different variants of the industrial heat pump and the SHARC designs at baseline conditions is presented in the sixth chapter. Two intercooling methods of the industrial heat pump including spray water and heat storage were compared. Then, a special design of steam generation without using a heat-pump cycle was investigated. For the SHARC system, two variants with differences in the steam extraction architecture were analyzed and compared in terms of thermodynamic performance.

Based on the results of the previous chapters, the final design of the complete system is presented in chapter seven. A brief description of the design is given and the thermodynamic performance in terms of power consumption and exergetic efficiency is

reported in this chapter. The investigation of the comparison between this system and a previous combined system of CO₂ based heat pump with Carnot battery is also shown.

Finally, the conclusion is given in chapter eight, which reports the most important findings. The last chapter discusses the potential developments that could be performed in later studies.



Vietnamese-German University

2. Theoretical background

2.1. Heat Pump principle

A heat pump main purpose is to transfer heat from a low-temperature source to a high-temperature sink. The second law of thermodynamics state that heat cannot flow from low to high temperature. However, mechanical work is utilized in a heat pump cycle to overcome this. In a heat pump cycle, medium fluid acts as heat carrier by flowing through the entire system. The overall process in a heat pump is as follows: the fluid absorbs heat at the low-temperature heat source, then it is compressed by a compressor before discharging useful heat at the high-temperature heat sink, and finally expanding before reaching the heat source to create a complete cycle.

Different variants of heat pump exist to accommodate various purposes, but the working principle does not change. These variants can be categorized based on the employed thermodynamic cycle and their working fluids [Gra 18]. Two types of cycles with common uses are discussed below.

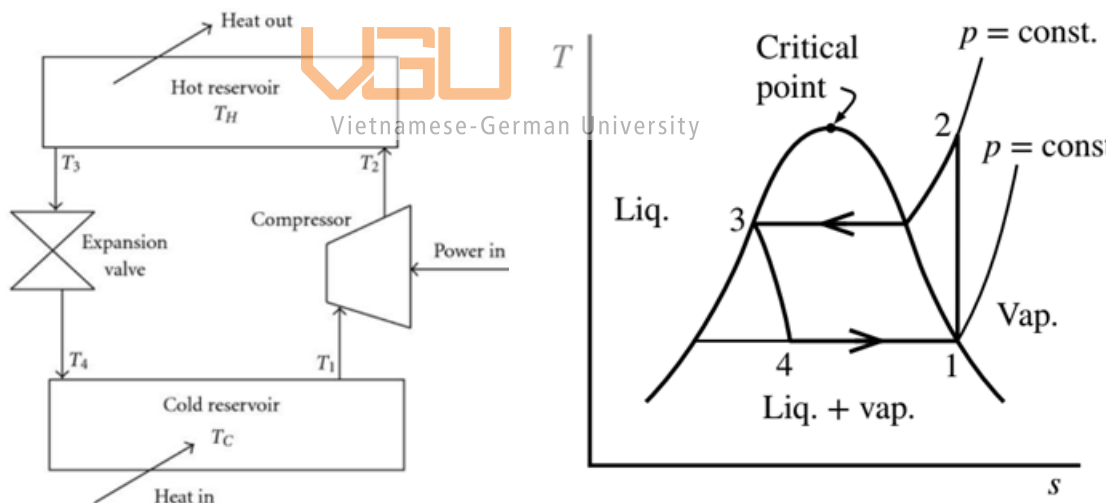


Figure 2.1.1. Schematic of reverse Rankine cycle [HuAn 10] (Left) and T - s diagram of the reverse ideal Rankine cycle [McG 14] (Right)

In industrial and domestic application, heat pump system operates most commonly on the reverse Rankine cycle, or otherwise known as the vapor-compression cycle. The simple design and Temperature-entropy diagram (or T - s diagram in short) are shown in figure 2.1.1. The main characteristic of this system that distinguishes itself from the Brayton cycle is the utilized synthetic refrigerant as the working fluid and the occurrence of phase transition in the heat exchanger. While flowing through the condenser, the refrigerant

undergoes phase change from superheated steam to saturated liquid by releasing heat. On the other hand, cold low-pressure mixture of liquid and vapor receives heat at the evaporator and vaporizes.

Heat pumps that work on this cycle transfer great amount of heat that is suitable for large-scale applications. This is due to the fact that heat transfer occurs at constant temperature, meaning latent heat exchange processes happen at the sink and source. For domestic and industrial applications, this is advantageous since the available temperature range is usually limited and so, sensible heat is typically not viable. Additionally, this cycle uses expansion valve instead of turbine, which reduces the pressure and temperature of the saturated liquid. The usage of throttling valve is the only option, as liquid can damage and wear the blades of the turbine. Under the same output pressure and mass flow condition, a throttling valve produces higher outlet temperature due to its isenthalpic expansion nature compared to the isentropic process considered in expander. However, the greatest benefit of this valve compared to a turbine is the significant economic benefit, which is a major factor in commercial use.

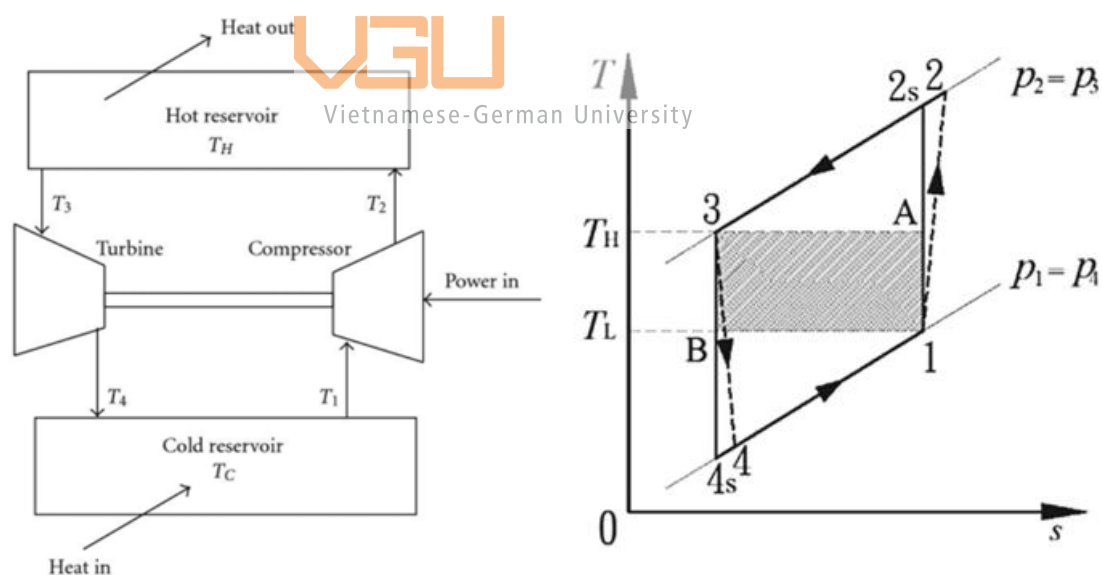


Figure 2.1.2. Schematic of a reverse Brayton cycle [HuAn 10] (Left) and T - s diagram of a reverse Brayton cycle [WaZh 18] (Right)

The other important thermodynamic cycle used in heat pump system is the reverse Brayton cycle, which is illustrated in figure 2.1.2. The differences of Brayton's cycle compared to that of Rankine's lie in the type of medium fluid and the phase of the fluid throughout the system. Air and some other gases are used as the working fluid instead of

synthetic refrigerants. Furthermore, no phase transition of the fluid occurs all over the system, hence the other name for this cycle is “gas cycle”. Therefore, the heat transfer mechanism here is sensible heat transfer, meaning heat supply and extraction from the system causes temperature change in the fluid.

Since the reverse Brayton cycle commonly uses air, it is typically implemented for aviation and modern gas turbine engine applications, where the supply of natural air is abundant [Hor 14]. It is commonly used to remove heat from certain parts of an aircraft, such as the cabin. The small refrigeration capacity per system size is also a reason for its usage in small-scale applications. As refrigerant only exists in the gaseous phase, it is feasible to use a turbine since it is more efficient and very low temperature level can be reached.

The use of natural air as medium fluid is very rare in industrial and domestic sectors, but its potential in these application areas, especially in residential and other heating services, has been investigated due to its environmental-friendly nature [WaZh 18]. However, this is not the scope of this paper.



Vietnamese-German University

2.2. State of the art

Heat pump is not a new technology, and it has long been employed in the industrial sector as a mean of heat recovery. Therefore, it is important that the state-of-the-art technology of the heat pump market is defined to ensure that this paper does not repeat on already existing work and can contribute to the uptake of heat pump in industry and future research.

Heat pump requires a heat source in order to operate, and industrial waste heat is a valuable supply due to its temperature range, which is higher than the ambient condition. It was reported that a temperature range from 30°C to 70°C was typical for industrial waste heat, with the maximum cases could be as high as 250°C [ABU+ 18], [MSZ+ 21]. For this paperwork, the heat supply extended from 30°C to 90°C, which corresponded to the current temperature range in industry. Specifically, three cases of inlet temperature were examined for the heat pump systems in this paper, including 30°C, 60°C and 90°C, which were the resultant outputs of different chemical processes. The low-grade heat

medium can be various, including flue gases, air, steam and so forth, which depends on the industrial process output.

More importantly, the operational temperature of heat pump, or in other terms the heat sink temperature, should be investigated. According to research on the current situation of heat pumps, commercially available industrial high-temperature heat pumps only operated in the range from 20°C to 100°C in terms of heat sink temperature by 2018 [ABU+ 18]. Heat pump models that can function at temperature up to 140°C were only prototypes created by pioneering manufacturers for demonstration. Above this temperature, research projects whose goal was to demonstrate sink temperature up to 200°C were still being conducted. The lack of heat pump system at higher temperature range was determined to be the results of many factors [ABU+ 18]. In general, one major cause is the information insufficiency in the market size and potential applications from the heat pump manufacturers [MSZ+ 21]. Other barriers included equipment costs, material restriction and lower efficiency at higher temperature with current technology [ZBB+ 19].

A techno-economic analysis on a heat pump system that operated with heat sink temperature at 280°C had already been accomplished [ZBB+ 19], which confirmed the feasibility of implementation at this temperature level. With the required output up to 300°C, it is not possible to design a completely practical system due to the absence of available heat pumps capable of accommodating such temperature. Instead, this paper only aims to provide a performance analysis of a theoretical system using simulation software provided by Siemens Energy AG. Thereby, it contributes to the expansion of the heat pump technology in temperature range higher than 200°C and further exploitation the potential of low-grade heat in a larger range of industries.

One other aspect beside the heat pump technology that should be considered is thermal energy storage (TES). The generated heat could be stored in thermal storage, to be discharged to generate electricity during the period when power demand and price is high. TES was expected to be a suitable integration to chemical industries, whose processes are energy intensive [CPE 12]. Energy efficiency improvement and greater cost savings are the major benefits of this integration. Various mechanisms of thermal storage have already been employed in correspondent to different sectors and conditions, especially in combination with heat recovery [ACC+ 16], [ZHX+ 14]. Molten salt TES was the

technology that had the most important characteristics of an energy storage system [ACC+ 16]. Specifically, it is economical, capable of providing grid energy storage and geographically independent. A system of combined heat pump cycle utilizing supercritical CO₂ and molten storage had also been developed. The upper limit for molten storage is 565°C, thus it is sufficient for a water-steam discharging cycle [ACC+ 16].

In summary, literature review showed that the potential of utilizing waste heat supplied from industrial processes were still considerable, whose typical temperature range was under 100°C. On the other hand, the heat sink temperature of up to 300°C, which was the target of this paper, was still not widely implemented. Therefore, these conditions would be the boundary conditions of the investigated system in this thesis. Additionally, the technology of TES, which was predicted to be beneficial if integrated with industrial sites, shall be examined in combination with the heat pump system.



Vietnamese-German University

3. Boundary conditions and requirements

The technical requirements and boundary conditions for the designed system were obtained from the reference paper of chemical sites [BPK+ 22] and are shown in the table 1. and 2. The system was demanded to work for a whole 24-hour duration, which will be discussed further in chapter eight.

Table 1. Requirements from the chemical sites

Requirements	
Electricity generation power	228 MW (24 hours)
Cold generation power	30 MW at -20°C (24 hours)
Low-pressure steam mass flow / Power	67 kg/s / 187 MW (24 hours)
Low-pressure steam temperature	200°C
Low-pressure steam pressure	6 bars
Medium-pressure steam mass flow / Power	60 kg/s / 176 MW (24 hours)
Medium-pressure steam temperature	300°C
Medium-pressure steam pressure	30 bars
Waste heat outlet temperature	20°C (winter) and 40°C (summer)

Vietnamese-German University

Table 2. Boundary conditions of waste heat and feedwater

Boundary conditions	
Waste heat inlet temperature	30°C - 90°C
Waste heat inlet pressure	4 bars
Feedwater temperature	15°C
Feedwater pressure	1 bar

The required properties of processed steam were different for each chemical process. For this paper's investigation, there were two output requirements that needed to be achieved, which were the low-pressure and medium-pressure steam generation. Specifically, the demands for the system were steam extraction at 6 bars and 30 bars, corresponding to the low- and medium- pressure categorization respectively. Also, temperature and mass flow for each category are specifically defined. Beside that, another required condition was set

for the outlet of the waste heat flow. At the cold side where heat is supplied to the system, the waste heat came in the form of liquid water as a by-product of chemical processes. Since water could reach a relatively low temperature due to heat extraction, it was deemed that the water flow should reach 20°C (for winter case) or 40°C (for summer case) in order to be reused in cooling towers. On the other hand, the requirement of cold generation was not realized but rather, it was assumed that the system used an artificial cold engine to satisfy this demand, which would be further discussed in chapter seven.

Three different levels of temperature for the water flow could be provided as products of various chemical activities, which were 30°C, 60°C and 90°C. The pressure of these heat sources were 4 bars. Feedwater that was used for steam generation entered the system at 15°C and 1 bar, which was at the ambient conditions.



4. Architectures of the investigated systems

4.1. Description of the investigated systems

For this thesis, two types of system were provided by Siemens Energy, which were the industrial heat pump design and the SHARC module. The stock designs were given as KRAWAL models. Then, they were redesigned into variants that could fulfil the demands from the chemical sites. The KRAWAL program shall be discussed in further details in section 5.2.

4.2. Industrial Heat pump

The purpose of this system is to generate steam at the required pressure levels. The system consists of two main sections: Heat pump cycle and steam compression module. It is to be noted that from this point onwards, the mention of “evaporator” and “condenser” shall refer to the components of the heat-pump cycle.

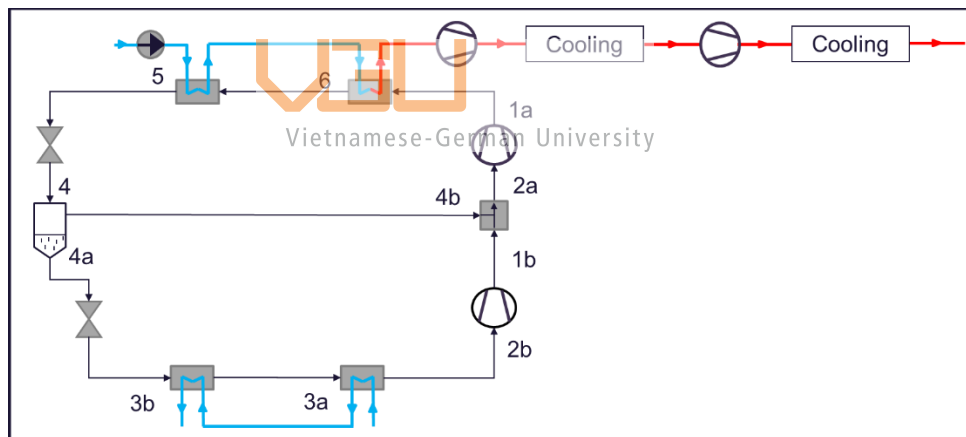


Figure 4.2.1. Schematic of industrial heat pump (Heat-pump cycle numbered)

The schematic of the heat pump is shown in figure 4.2.1. The heat pump cycle provides a large amount of useful heat by transferring thermal energy from the input to the output. The refrigerant is at its lowest temperature when it is absorbing heat at the source of the cycle ($5 \rightarrow 1a$). Firstly, the heat source provides heat to the system through an evaporator ($5 \rightarrow 6$) and a heat exchanger ($6 \rightarrow 1a$). Then, the refrigerant goes through a two-stage compression ($1a \rightarrow 2b$) with intercooling in between ($4b \rightarrow 1b$). The intercooling system

uses the low-temperature saturated vapor from the liquid-vapor mixture (4 → 4b) to cool the superheated refrigerant flow before entering the second phase of compression (1b → 2b). After that, heat from the resulting superheated gas is extracted through a condenser (2b → 3a) and a heat exchanger (3a → 3b) to heat up feedwater and create steam. Subsequently, the saturated liquid resulting from the heat extraction is throttled into the two-phase region, where the vapor is removed for intercooling (4 → 4a/4b). Finally, the remaining liquid is further throttled to a predefined evaporation pressure before once again supplied with heat, thus completing the heat-pump cycle.

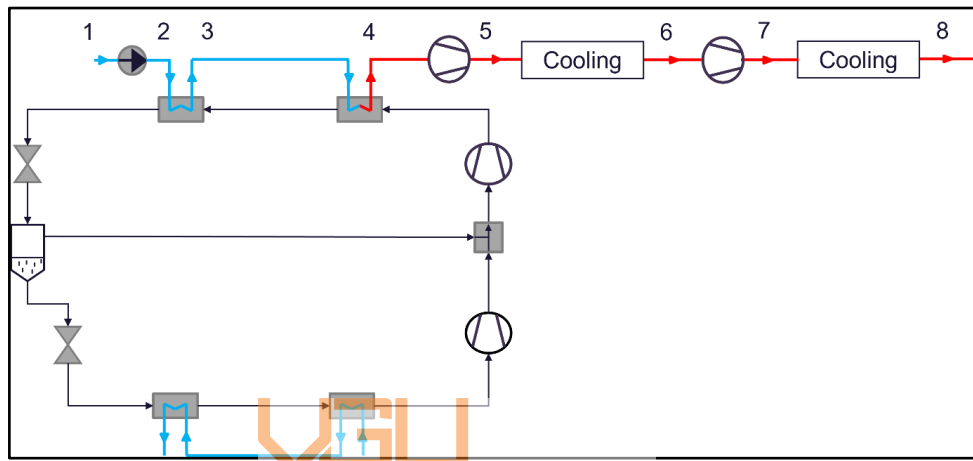


Figure 4.2.2. Schematic of industrial heat pump (Steam-compression module numbered)

On the other hand, the steam-compression module is an open system, in which the input is feedwater, and the output is high-pressure steam. Figure 4.2.2. depicts the numbering for the steam compression module. A small pump is used to transport water through the system (1 → 2). Next, the water flow is heated up (2 → 3) and evaporated (3 → 4) to produce low-pressure steam. A 2-stage compression process with intercooling is utilized to produce steam at the demanded pressure levels. Before reaching the end-use processes, the resulting steam flow is further cooled to reach the required temperature level.

The intercooling system is used in both the heat-pump cycle and the steam compression module. In the heat-pump cycle, the multi-stage compression process is used to raise the temperature of the superheated refrigerant by increasing its pressure level. Alternatively, the steam compression process' purpose is to raise the pressure to reach the demand requirements. However, the intercooling used in both sections helps reduce the compressor input power and thus improves the system efficiency. Additionally,

compression of steam would result in a higher temperature than required, so the cooling is used for lowering to a specified temperature at the output.

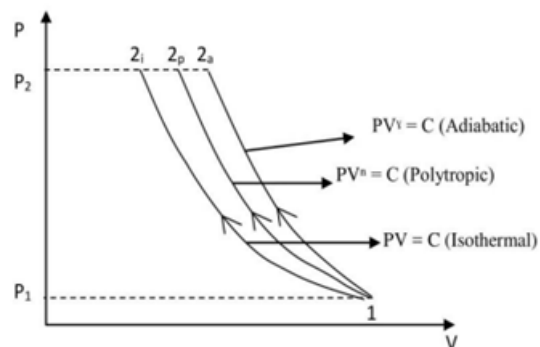


Figure 4.2.3. Pressure-Volume diagram of different compression processes [NLN 19]

The benefit of the intercooling mechanism can be explained through the use of a pressure-volume diagram (or p-V diagram) for different compression processes. The reversible work in an open system is described as

$$W_{rev} = \int_1^2 v dp$$

A reversible process is quasistatic, meaning a process that happens at very slow rate, so that thermodynamics parameters of the system could adjust to match the small changes from the process. Real life systems such as the one from this paper are never fully reversible due to dissipation in processes, which leads to irreversibility. However, formulas derived for the reversible process can still be used to analyze real life processes with enough assumptions. Here, the dissipation shall be neglected, and the reversible work is used for comparison between different processes.

Figure 4.2.3. depicts the p-V diagram of superheated refrigerant being compressed through three different processes, which are isothermal compression, multi-stage isentropic compression and single-stage isentropic compression from left to right respectively. Based on the formula, the amount of work supplied to (or extracted from) a process can be deduced from the area to the left of the p-v curve (blue and green shaded area in figure). For compression, isothermal process yields the best efficiency as it requires the smallest amount of work to compress. In practice, isothermal compression is not realistic as the process must happen very slowly to keep the fluid temperature constant by extracting heat from the fluid during compression. Instead, isothermal process only

acts as a limit for compression process [Bro 05]. Another process often considered in compression is the isentropic compression, meaning no heat is extracted and the refrigerant is reversible. Although no dissipation occurs, isentropic compression requires greater amount of energy due to its adiabatic nature. This is due to gas being heated up during compression and the volume increases as a result, thereby applying a greater back pressure on the compressor. In real-life application, the required power is even greater to compensate for the dissipation generated from friction, otherwise known as a polytropic process. Therefore, it is only reasonable to use a single-stage compressor if the poor performance can be neglected.

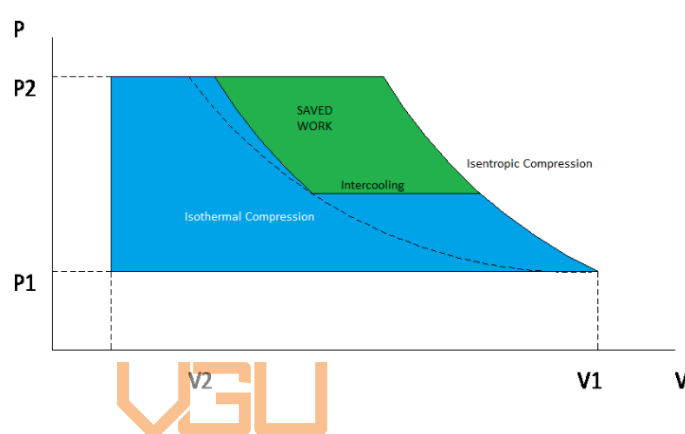


Figure 4.2.4. Pressure-Volume diagram of compression with intercooling [Cas 22]

The use of a multi-stage compression process with intercoolers helps minimize the required power, as shown in figure 4.2.4. Even though the compression at each stage is still polytropic, the cooling helps reduce the volumetric flow of the refrigerant flows at the compressor inlets, which results in lower compressor power. For greater number of stages there are in the compression, the closer the overall process will be to an isothermal compression and the lower the required power will be.

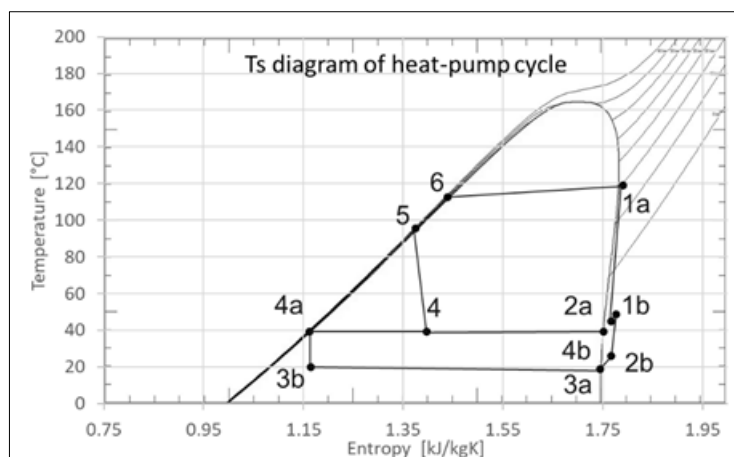


Figure 4.2.5. *T-s diagram of the heat-pump cycle at baseline conditions*

One additional benefit of intercooling is the reduction in the exergy loss produced during heat exchange at the heat sink. From the *T-s*-diagram in figure 4.2.4., the flow of cooler saturated gas mixed (4b) with the refrigerant flow after the first compression stage (2a) allows for a drop in entropy and temperature as heat is transferred to the cooler flow (1b). This in turns means that the refrigerant vapor has a smaller steam quality and is closer to becoming a saturated gas. Hence, the superheated vapor produced after the second compression stage is also nearer to the saturated line. Consequently, the exergy loss in the heat sink is minimized as the amount of required desuperheating is smaller and the heat exchange occurs mostly through phase change.

4.2.1. Intercooling with spray water

The cooling system for steam compression could employed two different designs. The first design uses a similar mechanism to the heat pump cycle as depicted by figure 4.2.5. A portion of low-temperature water from upstream is sprayed into the superheated steam flow during and after the compression process. The main goal for the intercooling system was to reduce the required power for compression. Furthermore, the spray water at the downstream adjusts the steam flow to the demanded temperature.

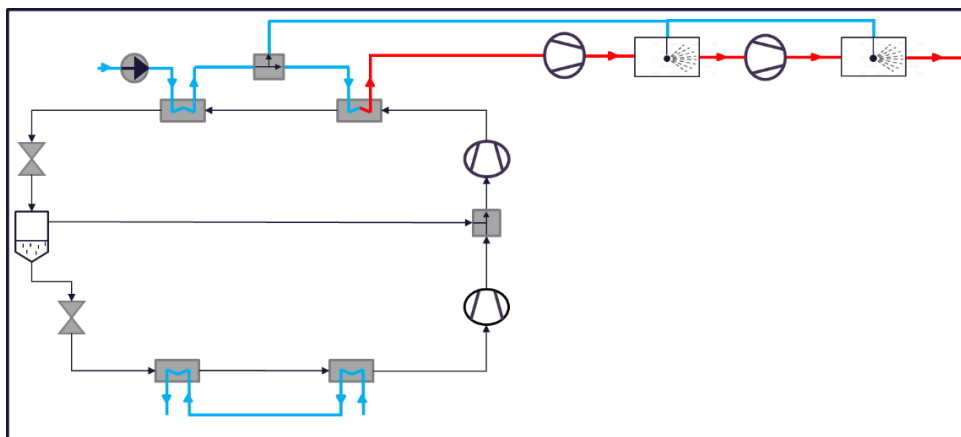


Figure 4.2.6. Schematic diagram of industrial heat pump with spray water intercooling

4.2.2. Intercooling using heat storage

Another considered mechanism for cooling was heat storage, as shown in figure 4.2.6. The idea of this design was mainly the utilization of unused heat during the cooling process, which would otherwise be wasted. The steam temperature is hot enough that heat can be extracted from it for storing and further used to generate more steam or electricity if a power cycle is included. Expectation for this design was the same or lower COP but higher exergetic efficiency due to the additional energy flow generated from the wasted heat, although there are additional losses in the heat exchangers used for cooling.

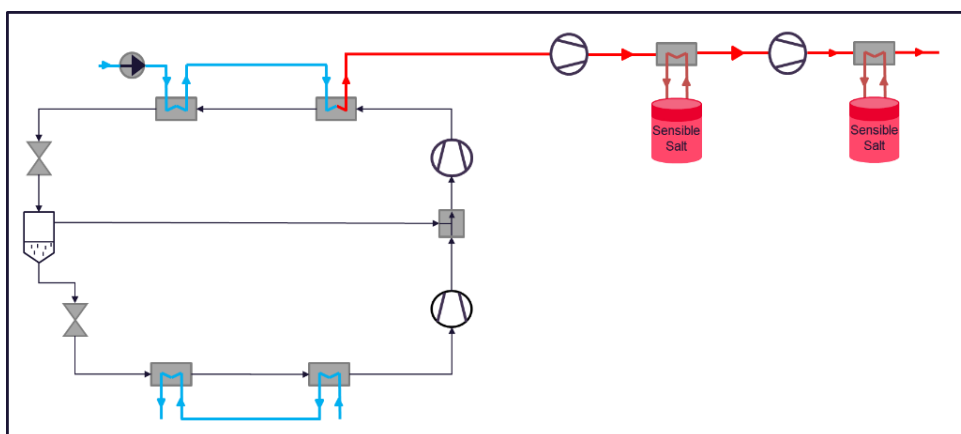


Figure 4.2.7. Schematic diagram of industrial heat pump with heat storage intercooling

4.3. Direct steam evaporation design

A special design, whose schematic is displayed in figure 4.3.1., was considered for the waste heat case with the inlet temperature of 90°C. At ambient condition, water evaporates at 100°C. Therefore, it is possible to generate steam directly from this heat source by lowering the evaporation pressure, hence lower temperature is required for vaporization. A KRAWAL model was produced such that the waste heat flow exchange heat with the water flow without a need for a heat pump cycle. Thus, this design goal was the reduction in terms of component and power consumption.

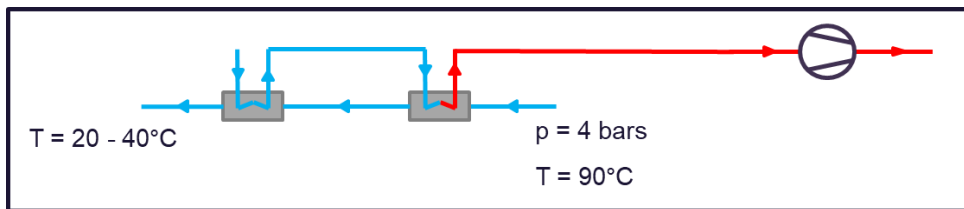


Figure 4.3.1. Schematic of direct steam evaporation design

4.4. SHARC design



The final system that had been investigated was an internal design developed by Siemens Energy, which was called SHARC. The design consists of two cycles, called the Charging cycle (left) and the Generation cycle (right), which is illustrated in figure 4.4.1.

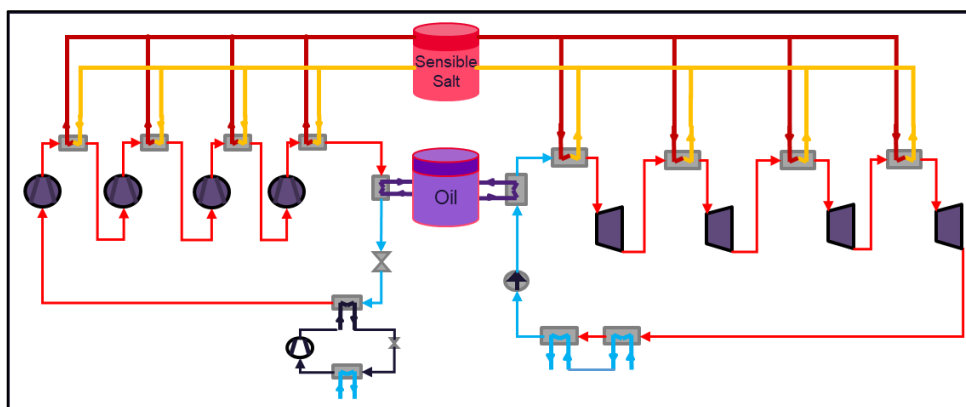


Figure 4.4.1. SHARC module with its Charging cycle (Left) and Generation cycle (Right)

SHARC is an abbreviation for “Storage H₂O Application Rankine Cycle”. Initially, the purpose of the system was the same as that of the Rankine cycle, which is to extract

mechanical energy from the fluid flow in the system for producing electricity. However, since the system operates on supercritical steam, it has the potential to generate processed steam that matches the required conditions from the chemical sites. Therefore, the SHARC design was also modified to generate both electricity and processed steam.

In the Charging cycle, thermal energy from waste heat is supplied by the implementation of a heat pump. This source of energy is then used for evaporating water in the cycle into superheated steam. After that, steam undergoes four stages of compression and heat extraction that charge a thermal storage which uses molten salt as its medium fluid and another heat extraction stage that charges an oil storage. From this point onwards, the heat exchangers that operate on salt and oil media shall be named as “Salt heat exchanger” and “Oil heat exchanger”. On the other hand, the Generation cycle utilized the stored thermal energy to heat up the steam medium so that it can be expanded when going through the turbines, which produces electricity. Therefore, SHARC design employs the principle of Carnot battery, in which electricity is stored as thermal energy. The intention is to operate the Charging cycle during the period when power price is low so that the storage can be charged. When demand increases and electricity price rises, the stored thermal energy can be converted back to electricity. In both cycles, the medium fluid of superheated steam can reach substantial levels of pressure and temperature, which is sufficient for the requirements of processed steam. For this paper, the extraction of steam from the Generation cycle has been investigated. Three possible variants of the Generation cycle had been developed and examined.

4.4.1. Additional turbines design

The first approach was to extract a partial load of steam from the generation cycle at baseline conditions and use the expansion process to convert it to the low- and medium-pressure steam requirements. Fig 4.4.2. depicts the T-s diagram for the generation cycle and the requirements for the processed steam, where the left red dot represents medium-pressure steam and the right one is for low-pressure steam.

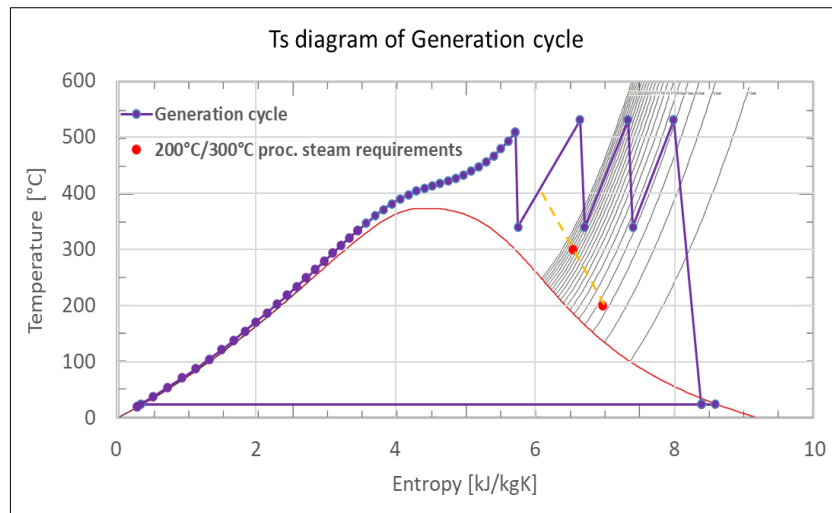


Figure 4.4.2. T-s diagram of SHARC's Generation cycle with single expansion line

Initially, a single expansion line was considered, which is expressed as the yellow dashed line in figure 4.4.2. Steam could be extracted from the second heat absorption stage of the Generation cycle and then expanded to medium-pressure and low-pressure level. However, it is shown in the diagram that such a process is not practical since the expansion slope was much steeper than a typical expansion process, which means that the isentropic efficiency of the turbine must be very low.

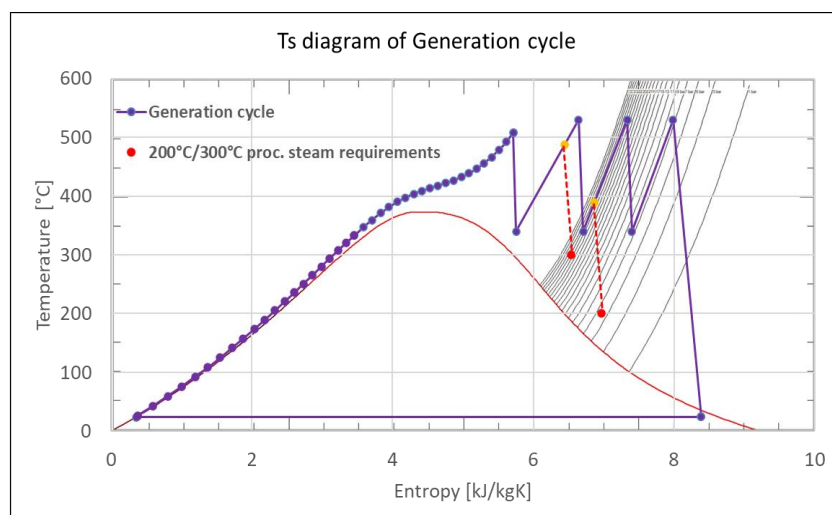


Figure 4.4.3. T-s diagram of SHARC's Generation cycle with double expansion lines

Therefore, the next logical step was to modify the system so that steam could be extracted and processed from two separate stages. The second and third heat addition stages were determined to be suitable for supplying the required steam. High-temperature steam from

each stage would then be expanded down to the required conditions, described by the red dashed lines in figure 4.4.3. This design was theoretically simple to create as no state variables of the Generation cycle, except for the mass flow, needed to be adjusted. Despite the feasibility of this system, further developments were not performed due to the complexity of the system, since at least two additional turbines need to be used for the extraction.

4.4.2. Steam extraction from second and third expansion stages

Instead of expansion, there were two other options for achieving the requested conditions of steam. From figure 4.4.4. which shows the generation cycle's temperature-entropy behavior at baseline conditions, it was determined that steam at the end of the second and third expansion stages were closest to the demand.

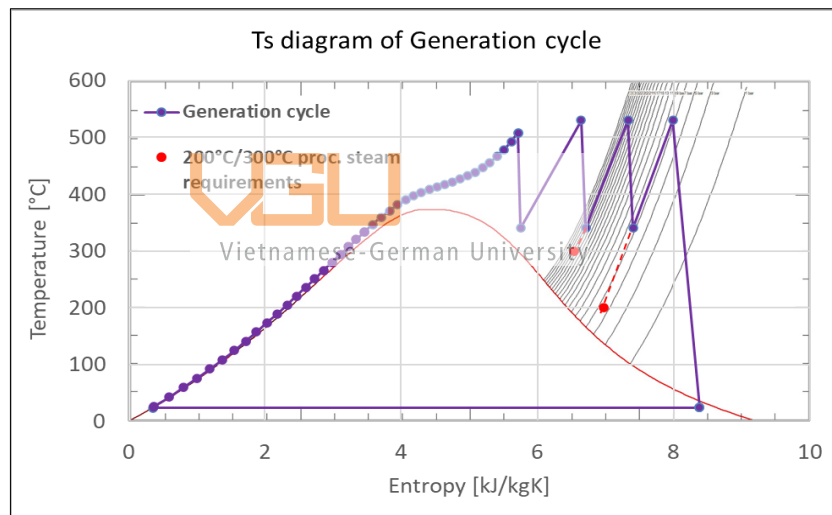


Figure 4.4.4. T-s diagram of SHARC's Generation cycle at baseline (for steam extraction from 2nd and 3rd expansion stages)

The first option was to adjust the cycle parameters so that the endpoints of the expansion stages matched exactly the low- and medium-pressure steam demands. This would be an ideal design since no additional components need to be incorporated into the system.

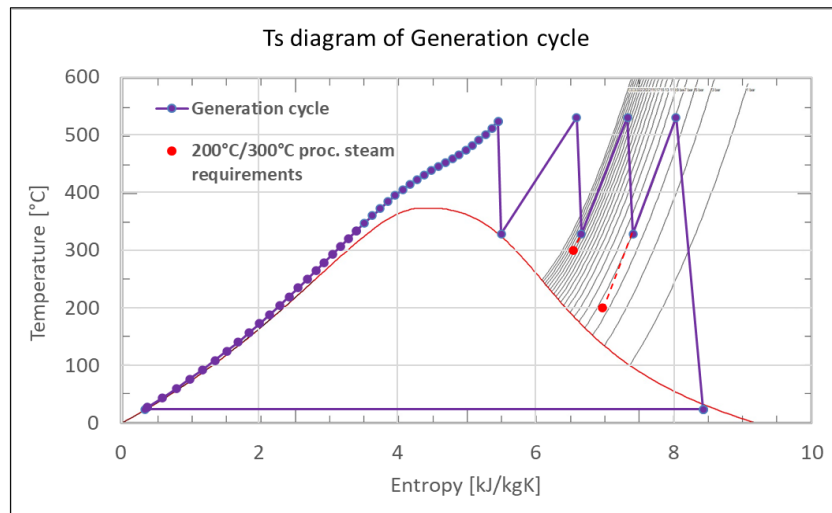


Figure 4.4.5. *T-s diagram of SHARC's Generation cycle at the adjustment limit (for steam extraction from 2nd and 3rd expansion stages)*

However, it was impossible to achieve this goal. Firstly, trying to adjust the cycle down to the low-pressure steam temperature of 200°C was impractical as the working temperature range of molten salt in the salt heat exchangers was from 345°C to 535°. Great temperature difference between the two fluids and the significantly lower temperature of steam would result in considerable exergy losses in the heat exchangers and thus poorer performance. In addition, the medium-pressure requirement could not be realized although it was closer to the Generation cycle in terms of pressure and temperature. The adjustment process of the Generation cycle was done as follows: The temperature after the second expansion stages was reduced with a small step size at a time (roughly 5°C) from the base temperature of 340°C, which led to a lower pressure level in the cycle; the pressure after the feedwater pump was adjusted to be greater to compensate for this and the steam pressure at output of 30 bars could be reached; then the process was iterated. However, the system reached its limit around 328°C of post-expansion temperature as shown in figure 4.4.5. From the diagram, it is shown that as the feedwater pressure increased, the four heat-supply and steam-expansion stages moved to the left towards the higher-pressure isobars. At the limit of 328°C, this pressure had already been required to be approximately 500 bars, which was impractical. Furthermore, the endpoint of the first expansion lies on the saturation curve for this case, meaning that further increment would lead to condensation in the turbine, which leads to the possibility of damaging the blades of the turbine.

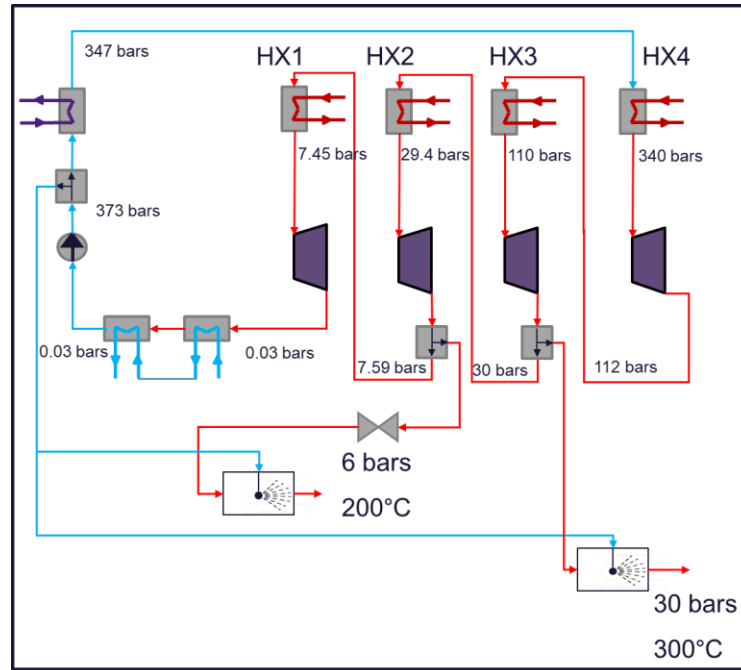


Figure 4.4.6. Schematic of SHARC's modified Generation cycle (for steam extraction from 2nd and 3rd expansion stages)

Because of the impracticability of the first option, the utilization of steam attemperation by spray water was investigated as the second approach. The schematic of the modified Generation cycle for this design is shown in figure 4.4.6. in which the temperature after all expansion stages were 340°C. At the endpoint of the second expansion stage, steam pressure was set to 30 bars to match the medium-pressure condition, so that the extracted steam was only needed to be isobarically cooled down to 300°C. On the other hand, the extraction of lower-pressure steam required an additional throttle valve since the pressure level after the third expansion stage could not be adjusted and was higher than required. The spray water was extracted from the upstream right after the feedwater pump. This design proved to be feasible and further investigations were performed to study the behavior of the system.

4.4.3. Steam extraction from first and second expansion stages

Another variant had also been created in which the main difference compared to the previous design lay in the different stages of steam extraction. For this system, medium-

pressure steam was extracted from the first expansion stage endpoint while low-pressure steam was extracted from the second.

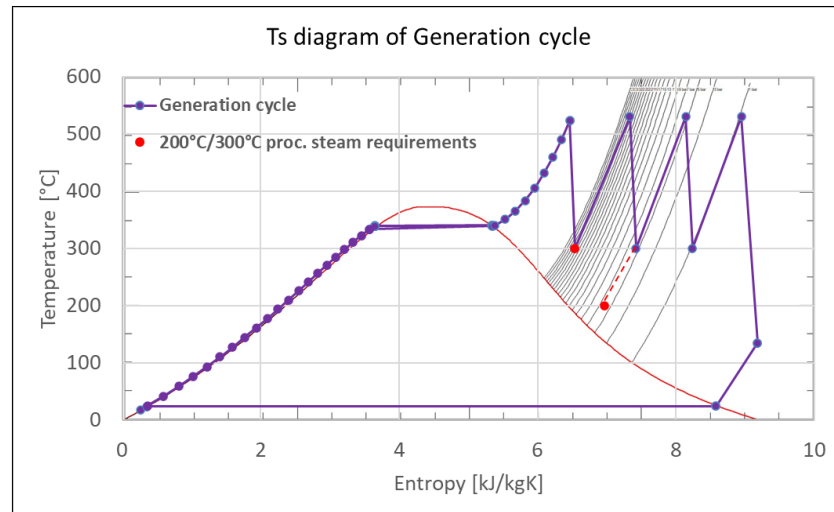


Figure 4.4.7. T-s diagram of SHARC's adjusted Generation cycle (for steam extraction from 1st and 2nd expansion stages)

From the T-s diagram shown in figure 4.4.7, the heat absorption and expansion stages shifted to the right compared to the baseline case, which meant that the overall pressure level in the system decreased. Therefore, this system was able to achieve matching conditions with the medium-pressure requirement since the pressure limitation from the previous design was not applicable here. However, since the overall pressure level decreased, water in the Generation cycle underwent a two-phase vaporization during the first heat absorption process in the salt heat exchanger. Due to this, it was expected that greater exergy loss would occur.

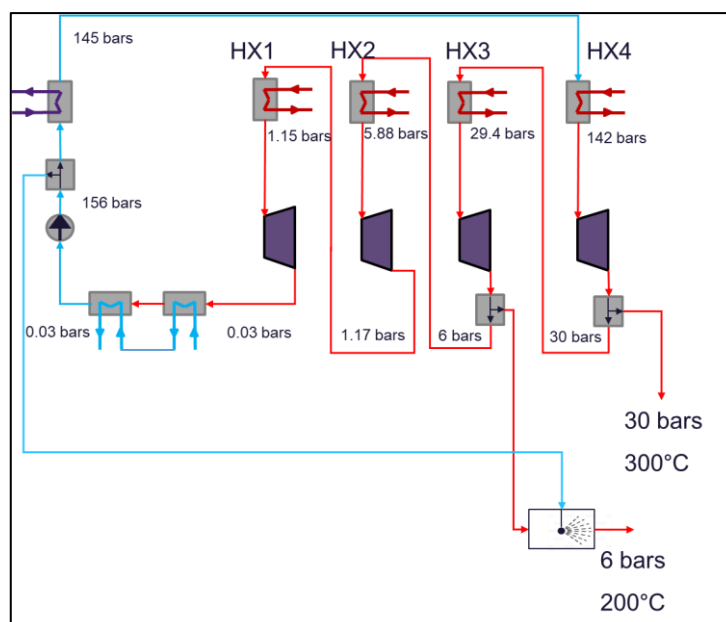


Figure 4.4.8. Schematic of SHARC's modified Generation cycle (for steam extraction from 1st and 2nd expansion stages)

The schematic for this variant is shown in figure 4.4.8. The mechanisms of steam extraction and attemperation by spray water were similar to the previous variant. The endpoint of the first expansion stage was adjusted to match the requirement of medium-pressure steam of 30 bars and 300°C. On the other hand, the steam pressure after the second expansion stage was set to 6 bars but the temperature was roughly 312°C, thus spray water must be used to cool down steam.

5. Constraint variation analysis

5.1. Description of constraint variation analysis

For real systems with many components, the degree of complexity can be significant and the relation between parameters in the system can be difficult to intuitively determined. Therefore, the constraint variation analysis serves as a preliminary step for understanding the behavior of the system with respect to the adjustment of certain constraints. In details, one constraint of the system, such as the evaporation pressure level of fluid, would be varied while all other parameters stayed fixed. The variation would be done over a predefined range with a constant step size. Data of the system would be recorded at each step size and shown together in graphs to display the trend of the system with respect to the variation.

The obtained results from this analysis could be utilized to predict the performance and requirements of the system under different boundary conditions, such as the summer case or the winter case. Moreover, optimization process of the system in further studies can reflect on this data as the theoretical framework. By understanding how a specific constraint affects the system performance, that constraint could be fine-tuned in the correct direction to get the most efficient design.

5.2. Methodology

5.2.1. System performance

To conduct evaluation for each variant, some parameters were chosen to be the characteristics for comparison. From a thermodynamics aspect, there are different efficiencies that can be used to assess the performance of a system. These efficiencies are generally defined based on the ratio between “benefit” and “effort” in a system. “Benefit” is the quantity that is considered to serve the purpose of the system (e.g. generated power in power cycle), whereas “effort” is the input amount that is expended to create the “benefit” (e.g. fuel combustion in engines). For the system presented in this paper, the “benefit” was considered to be the extracted useful heat in the form of superheated steam and generated electricity. The amount of supplied power to the system was instead deemed to be the “effort”. The following parameters are expressed based on this definition.

For a heat-pump cycle, the Coefficient of Performance (COP) is the foremost ratio that describes the effectiveness of the system. It is represented as follows

$$COP = \frac{\textit{benefit}}{\textit{effort}} = \frac{|\dot{Q}|}{P}$$

Where Q is the amount of extracted heat flow and P is total power consumption, both of which are in MW. Since the system produce steam, Q was regarded as the total amount of power and heat converted to thermal energy in the steam flow. A higher COP means that less work is needed to generate the same amount of heat flow at the sink and thus, lower operation costs.

In addition, the exergetic efficiency was also utilized for the evaluation of each concept. It is defined with the same principle but using a different property of energy

$$\eta_{ex} = \frac{\textit{benefit}}{\textit{effort}} = \frac{\Delta\dot{E}}{P}$$

Where $\Delta\dot{E}$ is the change in the exergy flow of the steam and P is the total power input. The exergetic efficiency is important as it considers the irreversibility of processes in the system, which compares the actual performance of the system to its reversible version. During thermodynamics process such as heat conversion, a portion of the total energy may be destroyed due to dissipation. The remaining amount of energy that can still be converted into useful work or heat is called exergy, which is also the property used in the calculation of exergetic efficiency. The “benefit” was the added exergy flow to steam while the amount of power fed into the system was again the “effort” since electricity or mechanical energy is considered to have no losses during conversion.

In summary, two parameters were used as the scale for comparison between different system variants. The COP was utilized to compare the amount of produced thermal energy in terms of high-temperature steam for the same consumed amount of power. Additionally, the quality of the extracted steam, or the portion of thermal energy that could still be converted into other useful forms of energy per input power unit was described by the exergetic efficiency.

5.2.2. Data collection method

Siemens Energy AG had developed a thermodynamics calculation tool called KRAWAL for internal usage. At the simplest level, KRAWAL is used for computing the state variables of a thermodynamic system or process given sufficient set of constraints and the design of the system, which is represented as connection of “aggregates” in the program. The constraints are parameters of the working fluid such as temperature, pressure, or the type of fluid itself, whereas “aggregates” are the components in the system that operate on or are operated by the fluid such as compressors, heat exchangers and so forth. The sets of constraints and aggregates define a system of equations that are derived from thermodynamic relations and laws. By solving these equations, the whole system can be fully defined. It is essential that the number of equations, which is established by the set of constraints, matches the system degree of freedom in order to compute all of the unknown values.

Then, the values obtained from the computation of KRAWAL was extracted to Excel datasheet automatically using a VBA macro, which was also developed by Siemens. For each variant calculation, the same procedure was done similarly, and Excel was used as the database. Additionally, other system parameters beside the obtained values from KRAWAL were computed by setting up automated functions in Excel. Finally, graphs were created using Excel to visually compare the variants.

5.3. Constraint variation analysis of industrial heat pump

5.3.1. Steam evaporation pressure

One of the parameters that required analysis to understand its effect more clearly was the evaporation pressure of the steam flow, which is indicated in figure 5.3.1. For the initial anticipation, this parameter was closely related to the required amount of power for compressors and pumps in the system. Thus, this analysis aimed to determine the magnitude of change in the system performance with respect to the variation of the pressure.

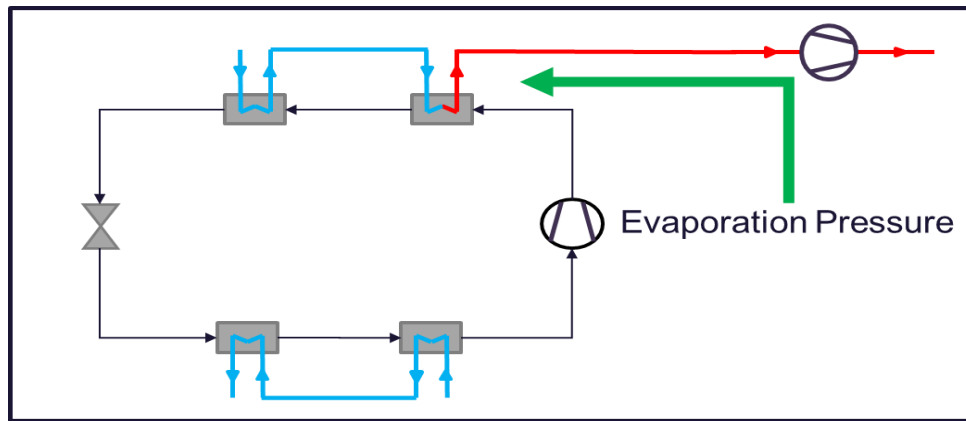


Figure 5.3.1. Schematic of industrial heat pump with indication of steam evaporation pressure

Specifically, it was expected that the steam evaporation pressure was proportional to heat-pump cycle compressors power and feedwater pump and inversely proportional to the steam compressors input power. For the compressors in the heat-pump cycle, the proportional relation between the required power and the pressure was attributed to the evaporation temperature of steam. If the pressure level at which steam evaporates got higher, then the required temperature for evaporation was also higher. Therefore, compressors must put in more thermal energy to heat the refrigerant to a greater temperature level. The reason for the correlation between the change in evaporation pressure and the feedwater pump was more direct. Since the heat exchanging process happens just after the feedwater pump, the evaporation pressure constraint directly determines the output of the pump. In contrast, the input to the steam compression module was controlled by the evaporation pressure. A higher input pressure meant lower power needed to raise the steam level to the demanded pressure. Overall, this means that the relation between the evaporation pressure and the whole system performance could not be intuitively determined since it was unclear which compression modules had the greater effect.

Thus, the procedure described in section 5.2.2. was used for the behavior investigation. In more details, the system was simulated under the same set of baseline conditions given in table 2., with steam evaporation pressure was the only changing variable. The pressure was varied from 0.35 bars up to 1.55 bars, with a step size of 0.1 bars.

Four cases of the industrial heat pump were developed in KRAWAL. The systems that utilize spray water and heat storage for intercooling each had two models for low- and

medium-pressure steam generation. For this variation, the results from the two steam output cases for each system were appropriately combined so that the whole system could be examined. For example, the COP was computed as the total extracted heat flow from the low- and medium-pressure steam output divided by the total power consumption in both cases.

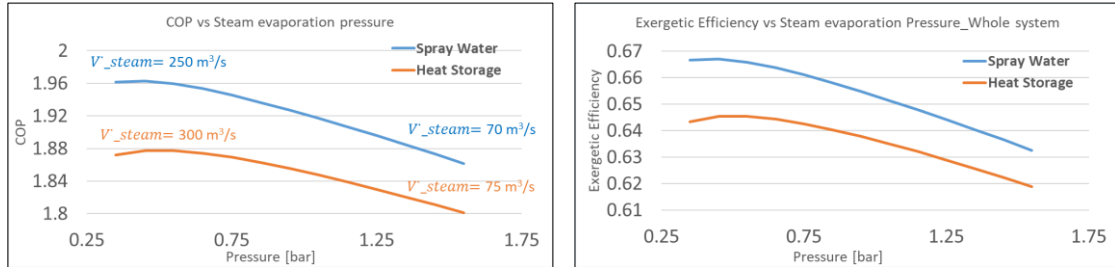


Figure 5.3.2. Industrial heat pump's (whole system) COP (Left) and Exergetic efficiency (Right) with respect to the variation of steam evaporation pressure

Results show that for the large part of the defined analysis limits, both systems performed better at lower evaporation pressure, as described in figure 5.3.2. The optimal point for efficiency was around 0.45 bars. In order to better explain this relation between the system performance and pressure, T-s diagrams of the heat-pump cycle were created for two cases of the production plant using spray water at low-pressure steam output.

The T-s diagram is useful for examining the heat transfer occurs in the cycle, which is a vital process of heat pump, since the area below the T-s curve is the amount of heat transferred to and out of the system. This is a result of the derivation from second law of Thermodynamics

$$ds = \frac{dq + (dw_{diss})}{T}$$

Where ds is the infinitesimal change of the fluid specific entropy, dq is the infinitesimal specific heat extracted or supplied to the fluid, dw_{diss} is the dissipated work occurs during the heat flow process and T is the thermodynamic mean temperature. A rearrangement of the second law gives

$$dq = Tds - dw_{diss}$$

Assuming the dissipation is neglectable, applying integral to both sides results in

$$\int dq = q = \int T ds$$

Thus, the amount of specific heat transferred from and to the system can be expressed by the integral of temperature and entropy $\int T ds$, which is the area below the T-s curve. Additionally, for a heat-pump cycle, the amount of work or power that is provided to the system can also be deduced as a result of the energy conservation

$$P = \dot{Q}_{out} - \dot{Q}_{in}$$

This means that the area between the temperature-entropy curve of the heat source and heat sink on the T-s diagram is the amount of power that must be supplied to the heat pump.

Other conclusions could be obtained from this diagram. For example, it shows that at lower steam evaporation pressure, the working fluid of the heat-pump cycle underwent smaller temperature change by throttling. The reason was due to the smaller temperature difference of the refrigerant between the evaporator and condenser, which was a result of lower condensing temperature of the heat pump fluid caused by the smaller steam evaporation temperature. As a result, there was smaller “required effort” in terms of throttling and thus, the dissipation occurred in the throttle valves was less serious. To quantify this loss, the property exergy could be utilized. Firstly, the change in exergy of a fluid flow could be defined as

$$\Delta \dot{E} = \dot{m} \cdot [(h_2 - h_1) - T_a \cdot (s_2 - s_1)] \quad [\text{CeBo 15}]$$

Since a throttling process is isenthalpic, the difference of the working fluid’s enthalpy before and after the throttle valve is the same. Hence, the change in exergy that happens during a throttling process is

$$\Delta \dot{E} = -\dot{m} \cdot T_a \cdot (s_2 - s_1)$$

The entropy of the fluid subjected to the throttling process always increases due to dissipation. From the formula, it can be concluded that the change in exergy of the mass flow is negative, or there is exergy loss. Therefore, this formula could be used to measure the amount of loss in a throttling process.

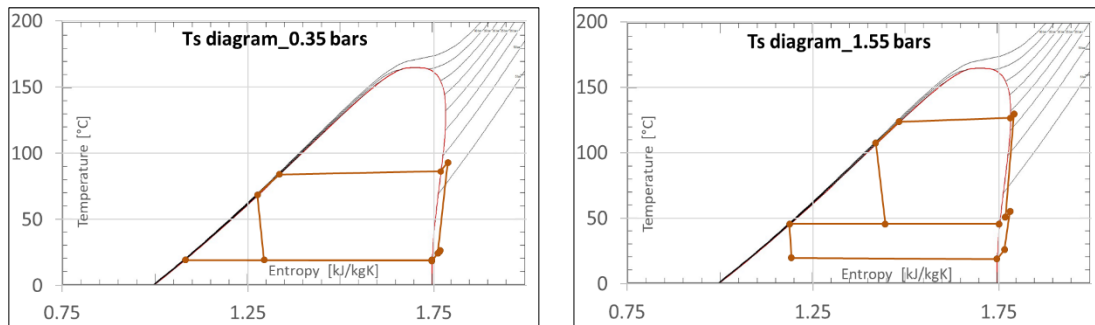


Figure 5.3.3. T-s diagrams of heat-pump cycle at steam evaporation pressure of 0.35 bars (Left) and 1.55 bars (Right)

From fig. 5.3.3., the entropy difference at higher steam evaporation pressure was greater, thus more exergy loss occurred at the throttle valves. A greater amount of input power must be supplied to the system to overcome these losses, meaning a slightly poorer performance at high evaporation pressure.

Additionally, the pressure ratio of steam compression in the heat pump was different for each case. The pressure ratio (or compression ratio) is the ratio between the pressure of the working fluid at the outlet to the pressure at the inlet of the two-stage compression, so a higher ratio means greater work must be performed by the compressors. As shown above, if the steam evaporation pressure was 1.55 bars, the temperature of R1233ZDE must reach over 120°C mainly through compression, which required the multi-stage compression to achieve a compression ratio of nearly 18. While for the lowest case of evaporation pressure at 0.35 bars, the ratio was just over 7.5, less than half of the previous case. Therefore, at lower evaporation pressure of steam, the supplied power to the heat pump compressors becomes less. However, the amount of heat transferred at the heat sink also reduces slightly since the temperature at which water evaporates is smaller and the mass flow is constant. This could be understood through the formula for heat transfer of heat exchanger

$$\dot{Q} = \dot{m} \cdot c \cdot \Delta T$$

Nevertheless, the significantly reduced amount of input power resulted in a higher internal COP of the heat-pump cycle, which were approximately 3.55 and 2.38 for the 0.35 bars and 1.55 bars respectively. For the overall scale of the whole system, the performance did not improve as greatly as the heat-pump cycle. This was due to the rise in pressure ratio of the steam compression module at lower evaporation pressure. Due to

this, the COP and exergetic efficiency of the system were limited to a maximum of 5% improvement only for the given range of evaporation pressure from 0.35 to 1.55 bars, where the optimal point was around 0.45 bars.

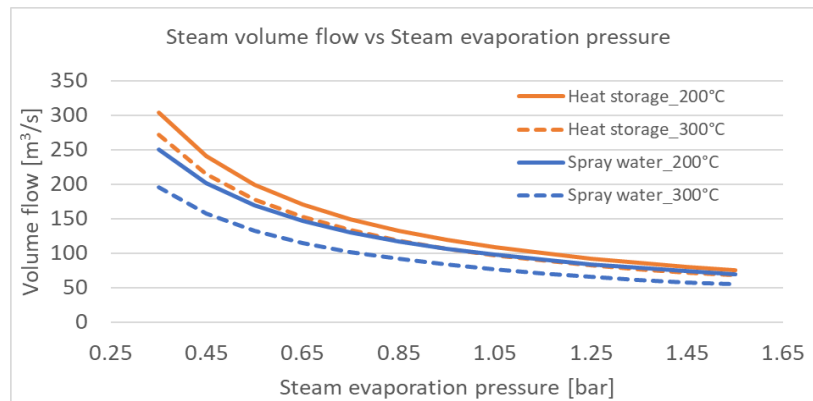


Figure 5.3.4. Industrial heat pump's volumetric flow of steam with respect to variation in steam evaporation pressure

However, some expenses must be satisfied in order to achieve lower pressure of evaporation. From figure 5.3.4, the required volumetric flow in the steam compression module, specifically for the section before the two-stage compression rose substantially as the evaporation pressure of steam decreased. Intuitively, as the pressure level was reduced, steam became less compressed and would expand, resulting in higher volume flow. This means that the geometric design of different components must be adjusted, for example the diameters of the pipe, to address this.

5.3.2. Waste heat inlet temperature

The inlet temperature of the heat source was the next parameter to be varied. In a study of heat-pump cycle conducted by Siemens Energy, a graph of theoretical COP change with respect to the heat source and heat sink temperature was created and is shown in figure 5.3.5 [Sie 22].

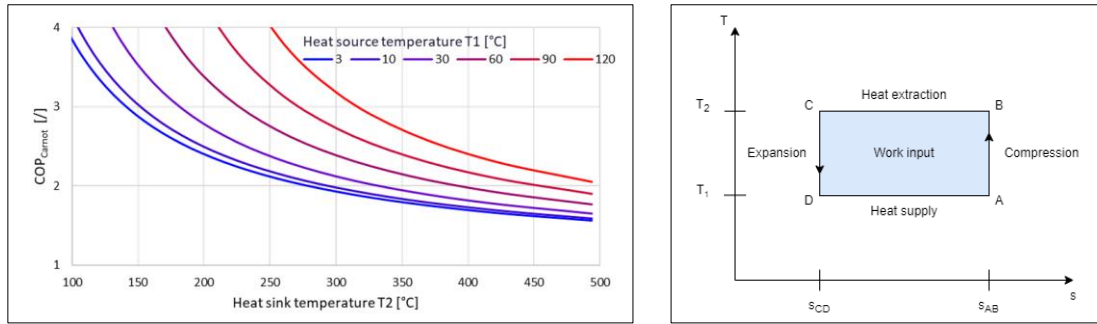


Figure 5.3.5. Theoretical COP of a heat pump with respect to heat source and sink temperature (Left) and T-s diagram of Carnot cycle (Right) [Sie 22]

The theoretical COP here is the maximally achievable COP where the heat pump operates on the Carnot cycle, which is a theoretical cycle, as shown in figure 5.3.5. This value is the upper limit for a heat-pump cycle operating at specific conditions and can be used to compare and predict the change in COP of heat-pump systems. The formula for this theoretical COP could be derived as follows

$$COP_{Carnot} = \frac{\dot{Q}_{out}}{P_{in}} = \frac{\dot{Q}_{out}}{\dot{Q}_{out} - \dot{Q}_{in}} \quad (1)$$

Where P_{in} is the amount of power supply to the heat pump, \dot{Q}_{out} is the heat flow at heat sink and \dot{Q}_{in} is the heat flow at the heat source. Due to the conservation of energy, the sum of heat and power supplied to the system is equal to the amount of heat extracted from it. From equation (1), the formula could be expanded as

$$COP_{Carnot} = \frac{T_2 \cdot (s_{AB} - s_{CD})}{T_2 \cdot (s_{AB} - s_{CD}) - T_1 \cdot (s_{AB} - s_{CD})} = \frac{T_2 \cdot \Delta s}{(T_2 - T_1) \cdot \Delta s} = \frac{T_2}{T_2 - T_1}$$

Where T_2 and T_1 are the temperature of the heat-pump fluid at the heat sink and source respectively. Therefore, the theoretical COP is only dependent on the temperature at the outlet and inlet of the cycle. For real cycles, there are always dissipation in components, causing growth in entropy and the system deviates away from the Carnot cycle. Hence, the behavior of the system does not follow this graph accurately, but it can be used to predict the direction and approximate the magnitude of change in the system COP for the case of temperature variations.

For this analysis, the heat sink temperature of the refrigerant could be considered as roughly 100°C, which was the evaporation temperature of water at 1.05 bars. The carrier of waste heat for this system was defined to be wastewater, the by-product of the chemical

processes. Additionally, three different levels of waste heat inlet temperature could be used to provide heat for the system, which were 30°C, 60°C and 90°C. The variant temperature levels corresponded to different processes in chemical industry, the most common of which was 60°C. Intuitively, a higher heat source temperature would allow for smaller amount of power input as more heat can be supplied to the system. However, it was considered necessary to analyze the sensitivity of the system performance relative to the change in heat source inlet temperature.

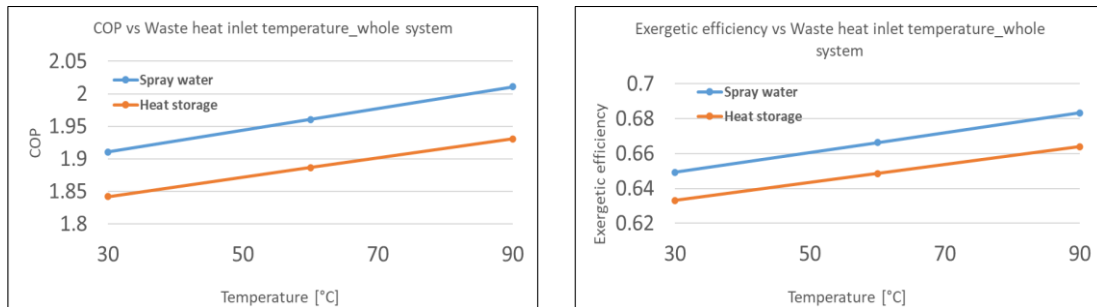


Figure 5.3.6. Industrial heat pump's (whole system) COP (Left) and Exergetic efficiency (Right) with respect to variation of waste heat inlet temperature

Figure 5.3.6 above show that at higher temperature, both the COP and exergetic efficiency of the system increased. Contrary to the prediction, the improvement of the system performance was not significant. Compared to the case with lowest temperature, both the COP and the exergetic efficiency at 90°C were only 5% greater than the 30°C case. For a Carnot cycle, the improvement of the theoretical COP, if the working fluid temperature increased from for example 30°C to 90°C, would be much many times greater than the obtained result. However, the considered system here included both the heat-pump cycle and the steam compression module, so it did not necessarily follow the predicted graph.

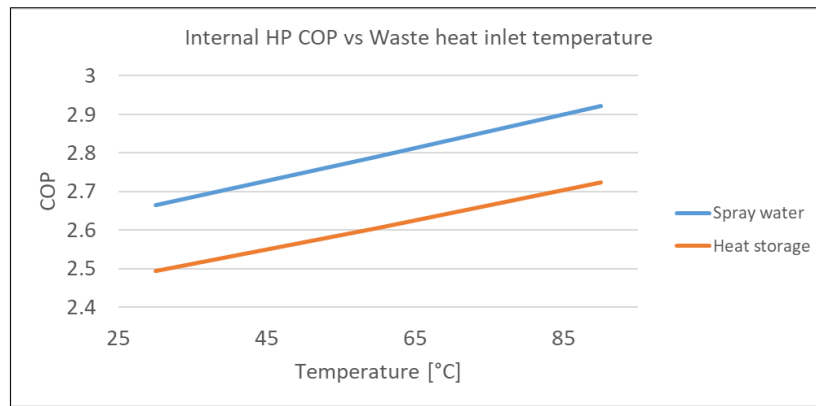


Figure 5.3.7. COP of the heat-pump cycle in the industrial heat pump system with respect to waste heat inlet temperature

The boundary conditions of the steam compression module would not change if the heat-pump sink temperature was modified. Therefore, the heat-pump cycle could be isolated and investigated to determine how it was affected by the change. Fig 5.3.7 shows the COP of the internal heat pump, which also increased as the temperature of wastewater rose. An improvement of nearly 10% was reported, which was two-fold of the similar figure for the whole system. Nevertheless, this was still unexpected since the result was many times smaller compared to the prediction.

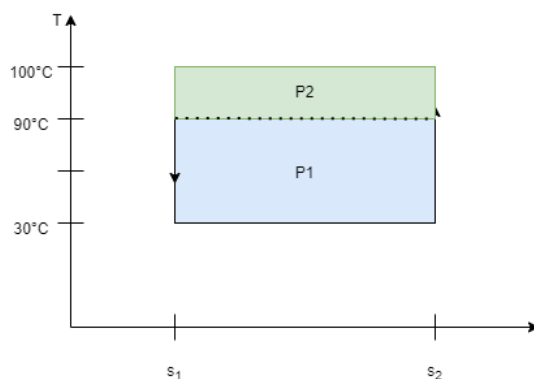


Figure 5.3.8. T-s diagram of Carnot cycle under the effect of medium fluid's evaporation temperature variation

Expectation was made that the evaporation temperature of the working fluid T_1 would rise proportionally to the increasement in wastewater inlet temperature as illustrated in figure 5.3.8. The input specific work P_2 of the case with 90°C inlet temperature would be smaller than with 30°C for the same output work, resulting in three times greater theoretical COP. Although the real system would not be able to reach this value due to

dissipation, the improvement was still expected to be significant, which was not the case. A closer inspection on the T-s diagrams of the heat-pump cycle's evaporator for the two cases of waste heat inlet temperature at 30°C and 90°C gave some insights.

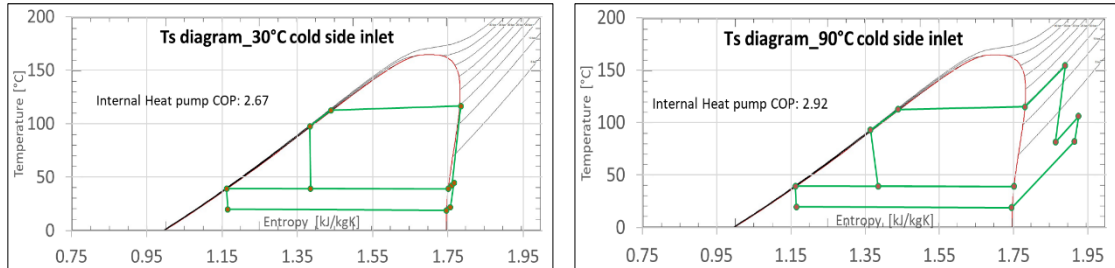


Figure 5.3.9. T-s diagrams of heat-pump cycle for the waste heat inlet temperature of 30°C (Left) and 90°C (Right)

Essentially, the most notable features of the two cases lay in the evaporator and the multi-compression stage. The diagrams from figure 5.3.9 show constant evaporation temperature of approximately 20°C for different waste heat inlet temperature cases. This was due to a constraint set on the temperature difference between the wastewater outlet and evaporation temperature, which meant that the evaporation temperature stayed the same since the outlet of heat waste was fixed to 20°C. Instead, KRAWAL utilized the higher temperature as additional thermal energy supplied to the system, which was manifested as the superheated fluid before the compression. Consequently, the COP did not increase significantly since the amount of input work did not decrease in folds according to the theory. Regardless, the extra heat supplied led to a reduced amount of required input power to generate the same amount of extracted heat flow at the sink, which in turn caused a better performance for the system at higher wastewater inlet temperature.

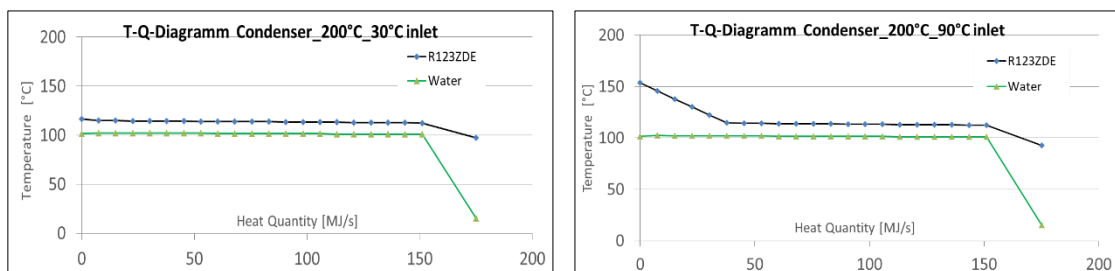


Figure 5.3.10. T-Q diagrams of the heat-pump cycle's condenser for the waste heat inlet temperature of 30°C (Left) and 90°C (Right)

The exergetic efficiency was an important parameter that needed to be investigated. Figure 5.3.6 shows that the efficiency also increased as the inlet temperature of wastewater was set to higher values, but the change was also only 5%. The heat pump was again investigated to determine the reason, in which the condenser and evaporator were focused. The results for the condenser from fig 5.3.10 show dissimilarities between the two cases. For the lower temperature case, the heat exchanging process at the condenser happens mostly through phase change, in which the temperature difference stayed almost constant. Meanwhile, the 90°C case results in a greater refrigerant temperature at the outlet of steam compression, leading to a greater desuperheating process before the latent heat exchange. For a heat exchanger, the exergy loss could be computed with the formula

$$\Delta \dot{E} = T_a \cdot \frac{T_H - T_C}{T_H \cdot T_C} \cdot \dot{Q} \quad (2)$$

Where T_a is the ambient temperature, T_H and T_C are the temperature of the hot and cold media respectively, and \dot{Q} is the heat flow. If the temperature of the fluids is not constant, the thermodynamic mean temperature shall be used instead

$$T = \frac{\Delta h}{\Delta s} \text{ Vietnamese-German University}$$

Due to the superheated steam at higher feedwater temperature, the heat exchanging process in the condenser contained a section where the temperature difference is greater, resulting in higher exergy loss.

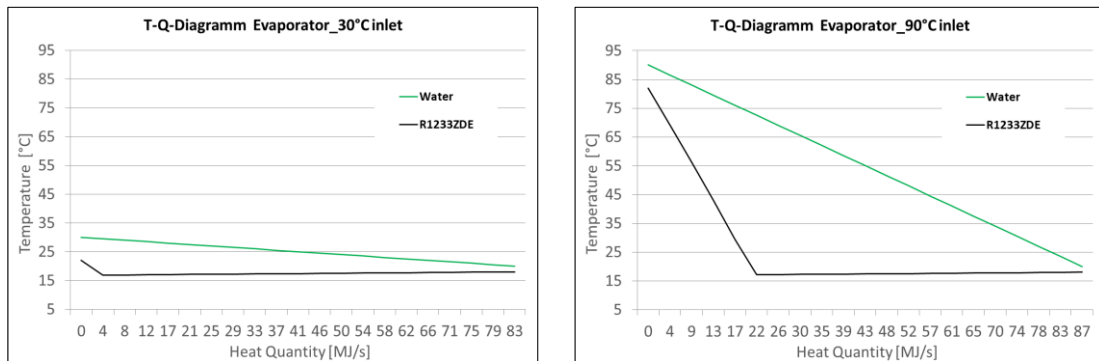


Figure 5.3.11. $T-\dot{Q}$ diagrams of heat-pump cycle's evaporator for waste heat inlet temperature of 30°C (Left) and 90°C (Right)

Similarly, the diagrams in figure 5.3.11. also show higher temperature difference in the evaporator due to the fixed value of output waste heat temperature but higher inlet

temperature. However, since the mean temperature of both fluids also rose, the exergy loss in the evaporator was hampered to a certain extent. Overall, the dissipation in the evaporator and condenser in combination with the throttle valves limited the improvement of exergetic efficiency.

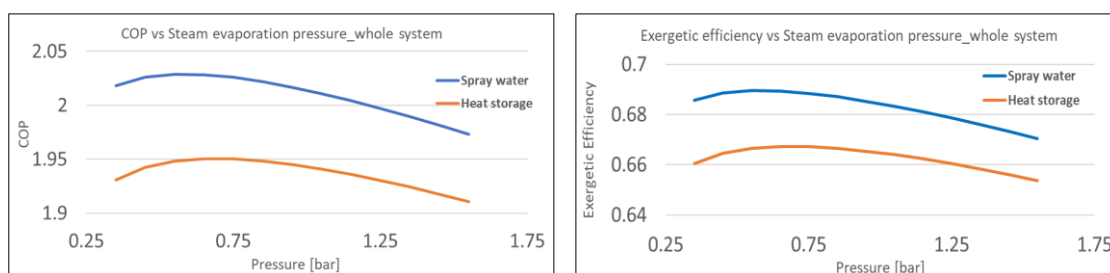


Figure 5.3.12. Industrial heat pump's (whole system) COP (Left) and Exergetic efficiency (Right) with respect to the variation of steam evaporation pressure at waste heat inlet temperature of 90°C

The next step was to vary the steam evaporation pressure to maximize the performance at 90°C. An analysis of the system performance for the pressure range from 0.35 bars to 1.55 bars was done. The graphs of the system performance for both designs are shown in fig 5.3.12. An optimal point of roughly 0.6 to 0.8 bars could be deduced from the diagrams. However, other factors must also be considered while determining the evaporation pressure. The change of volume flow in the compression module had the same behavior shown in figure 5.3.4., which shows that the required volume increased more significantly at lower pressure. Therefore, it was recommended that the pressure should be set to a value slightly greater than the optimal point. The exact value was not determined as it was not the scope of this paper.

5.3.3. Waste heat outlet temperature

As mentioned, the heat source could still be further utilized after supplying heat to the system. Specifically, the low-temperature water could be used in cooling towers to dispose unwanted heat from other processes. The required temperature of the wasted heat flow, or in this case the wastewater, changes depending on the season. Therefore, the analysis was conducted at the temperature levels ranging from 20°C (winter) to 40°C (summer) with a step size of 10°C. Other fixed constraints included waste heat inlet temperature of 60°C and evaporation pressure of steam at 1.05 bars.

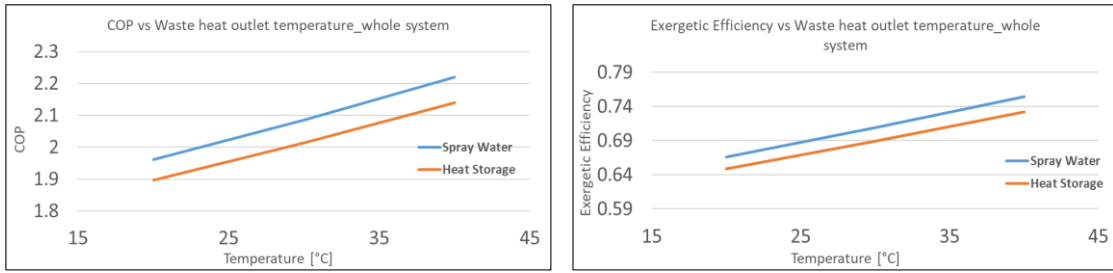


Figure 5.3.13. Industrial heat pump's (whole system) COP (Left) and Exergetic efficiency (Right) with respect to variation of waste heat outlet temperature

For the combined system of low- and medium- pressure steam output, its COP and exergetic efficiency were greater at higher temperature, which is described in figure 5.3.13. Particularly, the mentioned figures saw a nearly 13% increase from the lowest to highest temperature compared to roughly 5% in the previous variation. Hence, it could be expected that the system would perform better in the summer when the demand of the cold side was lower.

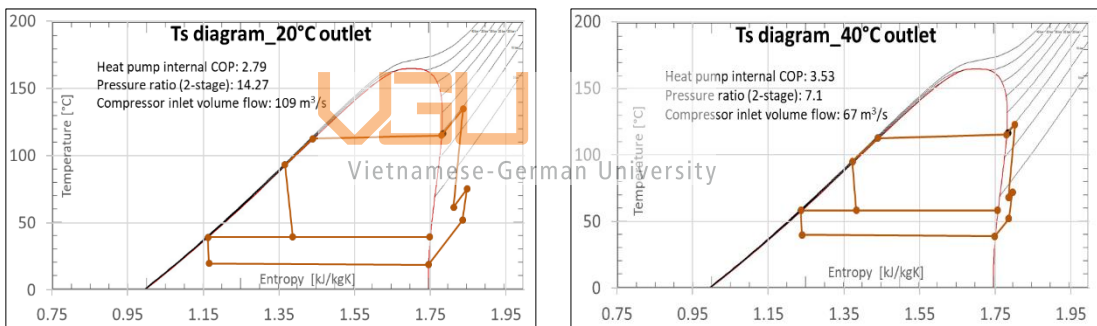


Figure 5.3.14. T-s diagrams of the heat-pump cycle for waste heat outlet temperature of 20°C (Left) and 40°C (Right)

The heat-pump cycle was again visualized in the T-s diagrams in figure 5.3.14. The diagrams illustrate the heat-pump cycle of the system with low-pressure steam output. A direct observation could be made that the evaporation temperature of the working fluid was higher in the 40°C case, which was not the case during the adjustment of the inlet temperature of waste heat. This temperature changed linearly with the wastewater temperature due to a constraint, setting the temperature difference between the outlet of wastewater and the inlet of fluid medium to be a constant value. As a result, the heat-pump fluid temperature was dependent on the wastewater temperature at the outlet.

In order to bring the evaporation temperature of the fluid to a higher level, its pressure of evaporation must also be greater. As a result, the pressure ratio of the cycle was smaller at higher temperature. The compressors thus required less power to compress the fluid to a certain pressure that was the same in both cases. Because the amount of heat flow extracted from the heat pump was the same in both cases, smaller compressor power resulted in greater internal COP of the heat-pump cycle, which is shown in the diagrams. Calculation showed an approximately 26.5% increase in COP of the heat-pump cycle from 20°C to 40°C waste heat outlet temperature, which matched more closely to the prediction of theoretical COP.

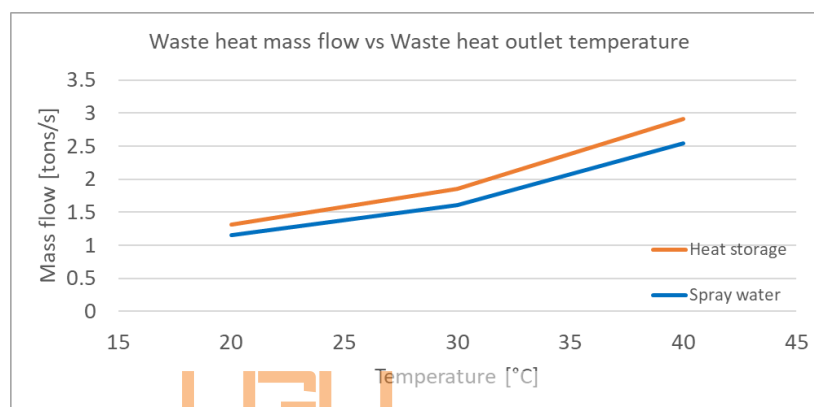


Figure 5.3.15. Mass flow of waste heat with respect to the variation of waste heat outlet temperature

Nevertheless, the amount of required wastewater flow is greater if the temperature at the outlet is higher, as displayed in figure 5.3.15. Since the inlet temperature was kept constant, the temperature difference between the evaporator ports would be reduced if the temperature of the outlet was increased. In order to keep the heat flow constant, wastewater must be supplied at higher mass flow rate.

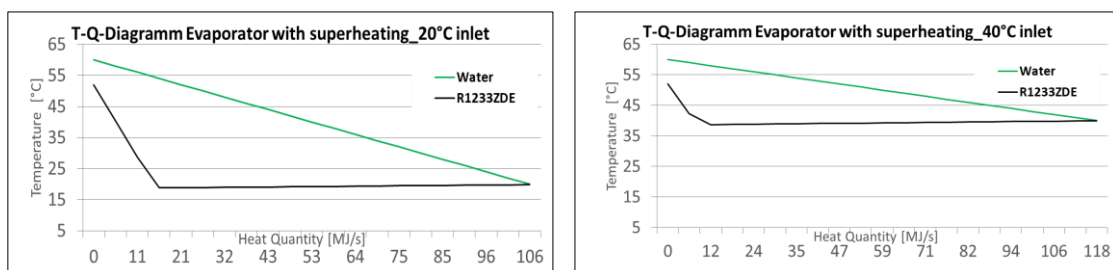


Figure 5.3.16. T- \dot{Q} diagrams of heat-pump cycle's evaporator for waste heat outlet temperature of 20°C (Left) and 40°C (Right)

In terms of exergetic efficiency, the system also performed better at higher temperature. The major distinction of the cycle for the two cases lay at the evaporation side. Therefore, the heat transfer process in the evaporator was analyzed using T- \dot{Q} diagrams in figure 5.3.16. Due to the smaller temperature difference, the exergy loss in the evaporator was also less significant for the case of 40°C. Additionally, the loss was further reduced due to higher mean temperature of the cold fluid, which could be concluded from the equation for exergy loss in heat exchanger (2).

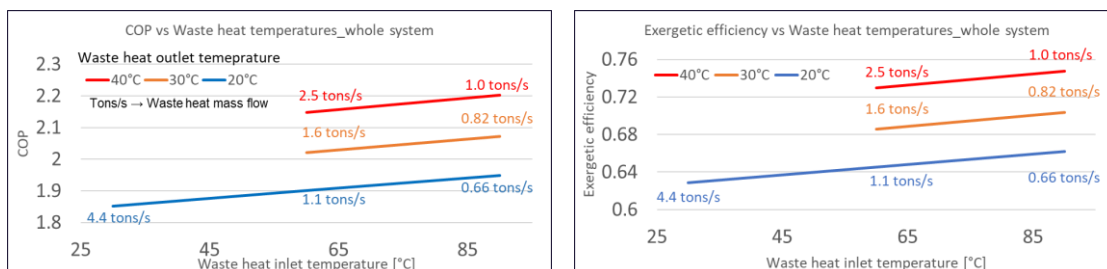


Figure 5.3.17. Summary diagrams for industrial heat pump's COP (Left) and Exergetic efficiency (Right) with respect to variation of waste heat temperature levels

In summary, the way the system changed with respect to the variation in waste heat temperature at both the inlet and outlet could be described by two diagrams in figure 5.3.17. The design with spray water for cooling was used to create these diagrams, since the other design with heat absorption for cooling showed the same behavior but poorer performance. Generally, the system was more efficient when the waste heat temperature at the inlet and outlet was higher. The required mass flow of wastewater was smaller for greater inlet temperature level. On the other hand, a greater amount of wastewater must be supplied to the system if the outlet temperature was high to provide enough heat flow.

5.4. Constraint variation analysis of SHARC design

5.4.1. Steam extracted mass flow

Steam extraction from second and third expansion stages

The first aspect that was worth investigating was the effects on the SHARC design as the extracted amount of steam increased. The analysis was conducted for isolated extraction from each expansion stage, meaning steam was extracted from only one expansion stage at a time.

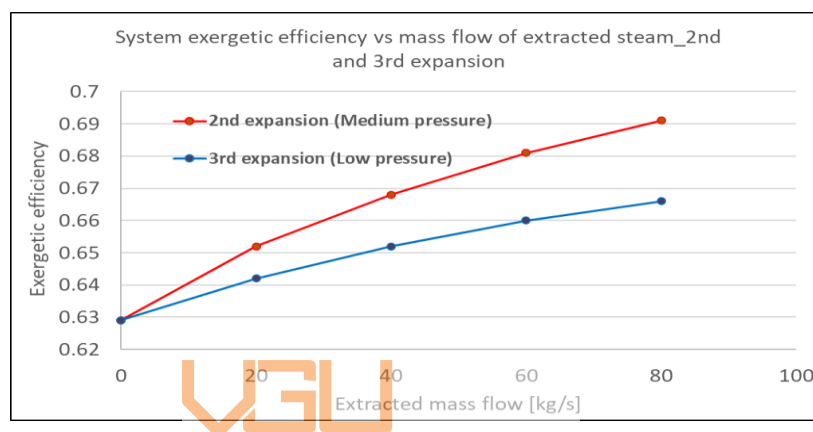


Figure 5.4.1. SHARC module's exergetic efficiency with respect to variation of steam extraction mass flow (for extraction from 2nd and 3rd expansion stages)

A step size of 20 kg/s and an upper limit of 80 kg/s were applied for this analysis, which resulted in the figure 5.4.1. The diagram depicts the system exergetic efficiency with respect to the amount of extracted steam variation. It is to be noted here that the efficiency did not consider the supplied exergy flow from the waste heat. This meant that the system benefited from greater exergy supply at higher amount of steam extraction, leading to a rise in exergetic efficiency.

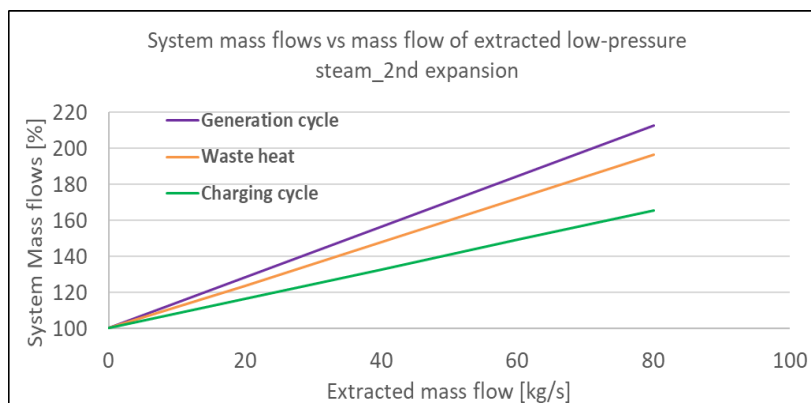


Figure 5.4.2. Relative change of mass flows in SHARC module with respect to low-pressure steam extraction from second expansion stage

At greater amount of extracted steam, the required mass flows in the Charging cycle, Generation cycle and waste heat rose. Figure 5.4.2 shows the relative rate of change of mass flows in the system with respect to the variation of medium-pressure steam extraction amount from the second expansion stage. The amount of supplied waste heat is an important parameter as it depends on the capacity of the end processes. At the upper limit, the required waste heat was already twice as much as the same figure at baseline. Also, greater mass flows in both cycles meant the scale of the system increased. Therefore, the limitation on the amount of steam production should be considered for each case.

Steam extraction from first and second expansion stages

The second variant saw the process of subcritical heat transfer in one of the salt heat exchangers. The T- \dot{Q} diagram of “Salt heat exchanger 4” in which the subcritical heat supply process occurred is shown in figure 5.4.3.

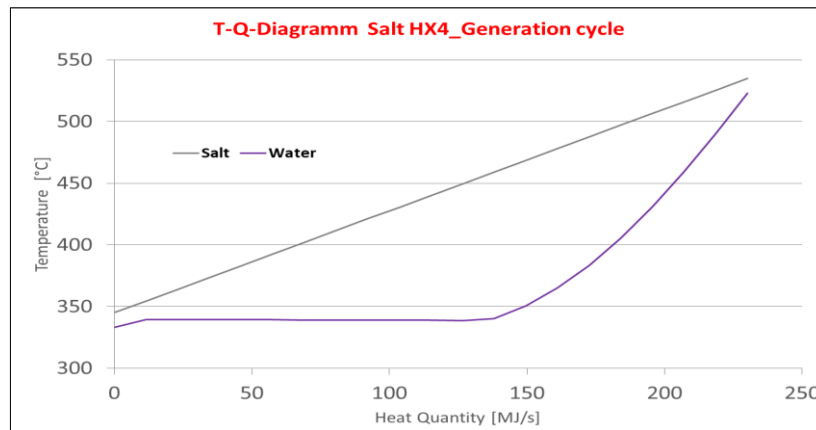


Figure 5.4.3. T- \dot{Q} diagram of "Salt heat exchanger 4" in the Generation cycle

Due to the constant-temperature process of water vaporization, the temperature difference between the two fluids increased significantly inside the heat exchanger. Compared to the sensible heat transfer processes for both fluids in the previous design, this system suffered from a higher reduction of exergy, which resulted in lower exergetic efficiency based on equation (2).

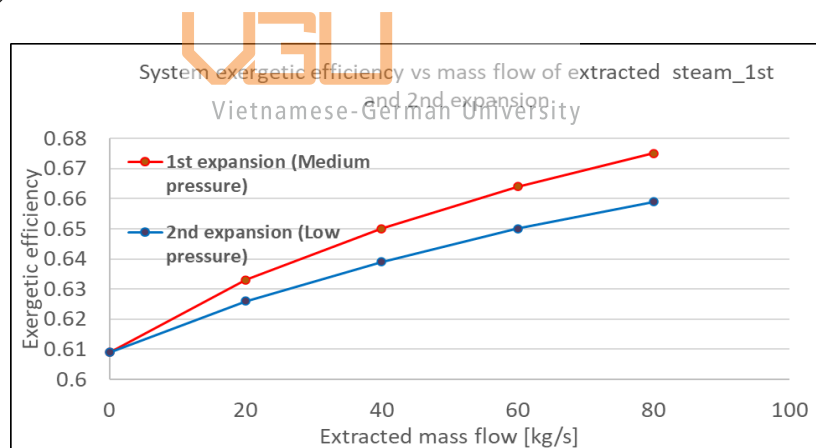


Figure 5.4.4. SHARC module's exergetic efficiency with respect to variation of steam extraction mass flow (for extraction from 1st and 2nd expansion stages)

A diagram representing the change of the system exergetic efficiency with respect to variation of steam extraction mass flow is shown in figure 5.4.4. The behavior of the efficiency and other parameters followed the same pattern as the previous design, thus further investigation for this system was not performed.

5.4.2. Waste heat temperature

Similar to the previous investigation with the industrial heat pump design, this analysis aimed to understand the behavior of the system with respect to the change in the waste heat temperature, both at the inlet and outlet. A summary diagram showing the exergetic efficiency of the system with respect to the corresponding inlet and outlet temperature of waste heat is shown in figure 5.4.5. The analysis was conducted on the variant that extracted steam from the second and third expansion stage.

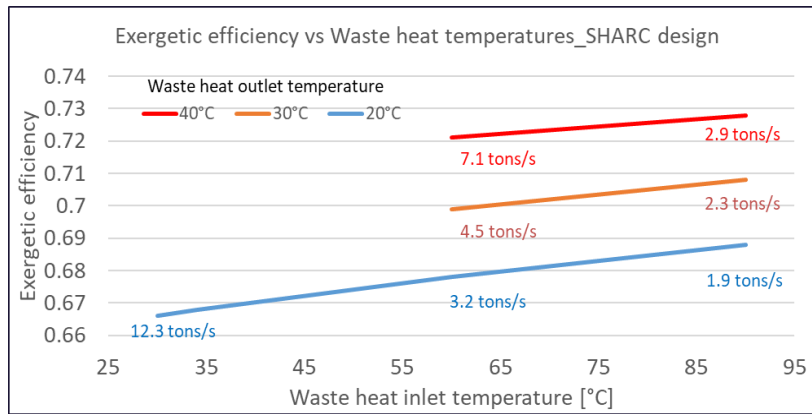


Figure 5.4.5. Summary diagram of SHARC module's exergetic efficiency with respect to variation of waste heat temperature

Vietnamese-German University

As expected, a similar pattern to that of the industrial heat pump system was reported. Increasing the inlet temperature of wastewater would lead to higher exergetic efficiency and lower required amount of waste heat. The exergetic efficiency would also rise with higher outlet temperature, but at the cost of greater mass flow of wastewater needed. Deeper analysis on the model showed that the variation of temperature did not affect the state variables of the Charging cycle and the Generation cycle, but only the heat-pump cycle got modified. Thus, the SHARC design saw the same behavior to the industrial heat pump since in both systems, only the heat-pump cycle changed.

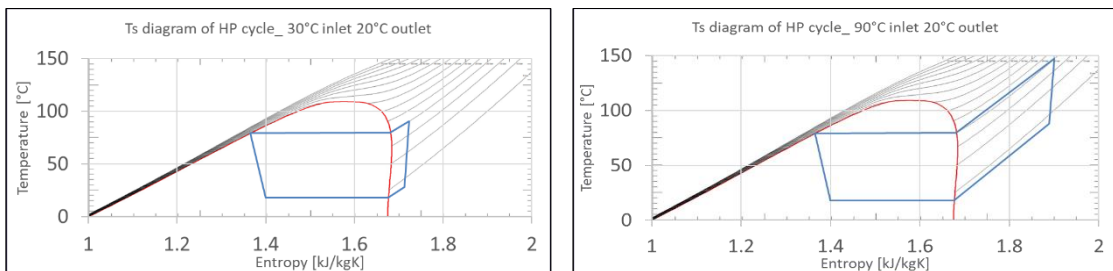


Figure 5.4.6. T-s diagram of SHARC's heat-pump cycle for waste heat inlet temperature of 30°C (Left) and 90°C (Right)

Figure 5.4.6 shows the T-s diagrams of the heat-pump cycle of the SHARC system for the case of 30°C inlet temperature and 90°C inlet temperature, both of which had the same outlet temperature of 20°C. The diagrams show that as the temperature level of the wastewater inlet increased, the evaporation temperature of the heat-pump medium did not rise. By contrast, additional amount of superheated fluid was created as a result, leading to greater performance at higher temperature.

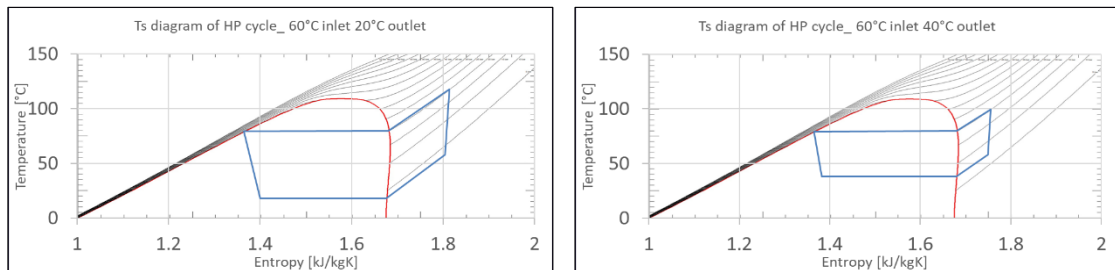


Figure 5.4.7. T-s diagram of SHARC's heat-pump cycle for waste heat outlet temperature of 20°C (Left) and 40°C (Right)

For the variation of the wastewater outlet temperature, the T-s diagrams of the heat-pump cycle were created for the cases of 20°C and 40°C outlet temperature in figure 5.4.7. In contrast to the variation of the inlet temperature, the adjustment of the outlet temperature resulted in different level of evaporation temperature of the heat-pump cycle fluid and thus, lower amount of exergy loss in the evaporator. Therefore, the exergetic efficiency would increase more significantly compared to the modification of the wastewater inlet temperature.

6. Comparison analysis of different systems

6.1. Comparison analysis description

The conclusion of the constraint variation analysis had provided insights into the different modules. However, this was not sufficient for choosing the most optimal variant for each module. Therefore, the performance comparison analysis was performed to compare the investigated variants. The variants in each module were compared under the same set of conditions. Most notable conditions were the temperature levels of waste heat, which were 34°C for the inlet and 20°C for the outlet. The exception was made for the design of no-heat-pump design, in which the inlet temperature was set to 90°C while the outlet was not fixed.

6.2. Industrial heat pump

6.2.1. Intercooling methods

The two mechanisms of intercooling for the steam compressions modules had already been described in section 3.1.1 and 3.1.2. The performance between these designs could already be deduced from previous analyses. Nevertheless, this section reports in more details the results of the thermodynamic investigation on these structures and possible causes for the outcome.

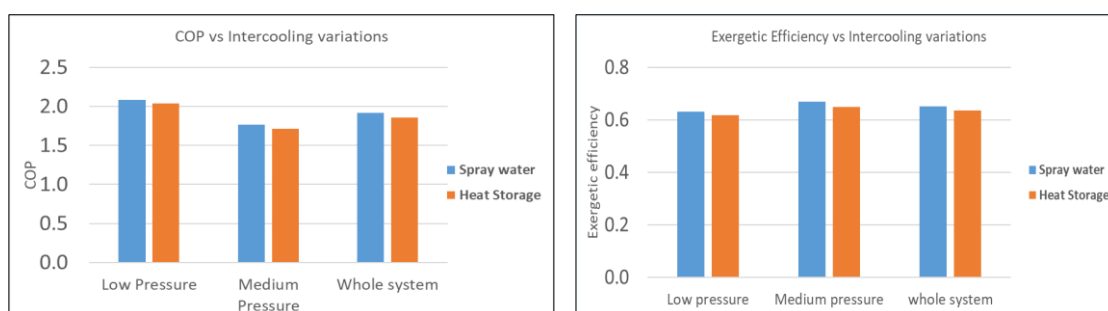


Figure 6.2.1. COP (Left) and Exergetic efficiency (Right) of variants of the industrial heat pump

The diagrams in figure 6.2.1. show the COP and exergetic efficiency of the whole system, meaning system with combined low-pressure and medium-pressure outputs, for each intercooling design. Results showed that the performance of the plant using heat storage as the intercooling method was slightly poorer than the spray water counterpart.

Although it was expected that the design with cooling using heat storage would obtain better result as greater amount of steam could be generated, the overall COP and exergetic efficiency were smaller than that of spray water. The amount of required power for compressors in both the heat-pump cycle and steam compression module were significantly greater to compensate for the additional amount of extracted heat. Moreover, the introduction of heat exchangers in the steam compression module further increased the pressure loss effect, which was assumed to be 2% in each exchanger. This meant that more power must be supplied to overcome this reduction of pressure.

For the analysis of exergetic efficiency, the quantity of exergy loss could be examined to justify the difference in performance between the two designs. It could be simply concluded that the reason for lower exergetic efficiency in the system with heat-storage cooling was due to the loss in the additional heat exchangers. In addition to the 2 heat exchangers that absorbed heat from the steam flow, another two exchangers must be used to evaporate extra steam for each output of low- and medium-pressure.

6.2.2. Direct steam evaporation design

The design with no heat-pump cycle was specifically created for the case with wastewater inlet temperature of 90°C. At this temperature, water can be evaporated if its pressure is slightly smaller than the ambient. This design brings benefits in terms of compactness and economics since only the steam compression module is needed. Moreover, the obtained results, which are depicted in figure 6.2.2, show that the system can be highly efficient if conditions were met.

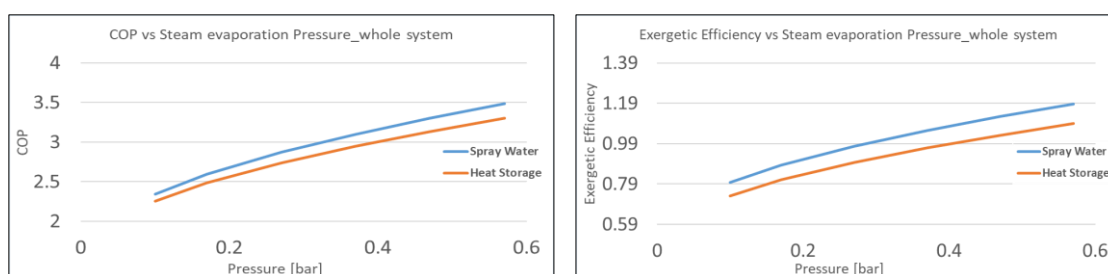


Figure 6.2.2. COP (Left) and Exergetic efficiency (Right) of direct steam evaporation design with respect to variation of steam evaporation pressure

A set of simulation was conducted for the range of evaporation pressure from the lower limit of 0.1 bars to the higher limit of 0.57 bars, in which steam could be directly vaporized by the flow of wastewater. For the initial observation, the obtained data of the system performance shows greater potential than the previous designs. Due to the exclusion of the heat-pump cycle, no power was supplied to transfer waste heat through the cycle. Therefore, the only amount of power needed by the system was for the compression module, which was comparably smaller than the provided heat. Since waste heat was not considered as the “effort”, this design benefited from the reduction of used power by utilizing waste heat as the main source of energy. Hence, the COP of the system was greater than the previous architecture with an internal heat pump. Similarly, the exergetic efficiency of the system also saw a much greater improvement, reaching an efficiency of nearly 1.2 at the upper limit. It is not possible to reach an efficiency higher than unity due to destruction of exergy in conventional heat pump. However, the supplied exergy flow of the heat source was not considered and the compressor power for the steam compression module was the only “effort” in the exergetic efficiency formula. As a result, the efficiency could reach a much higher level than usual systems.

Regardless, the model was unfeasible despite the huge potential for cost reduction and system compactness. One of the major boundary conditions that was deemed unable to be achieved with this design was the waste heat outlet temperature. Inspection using a $T - \dot{Q}$ diagram shows clearer cause for this limitation.

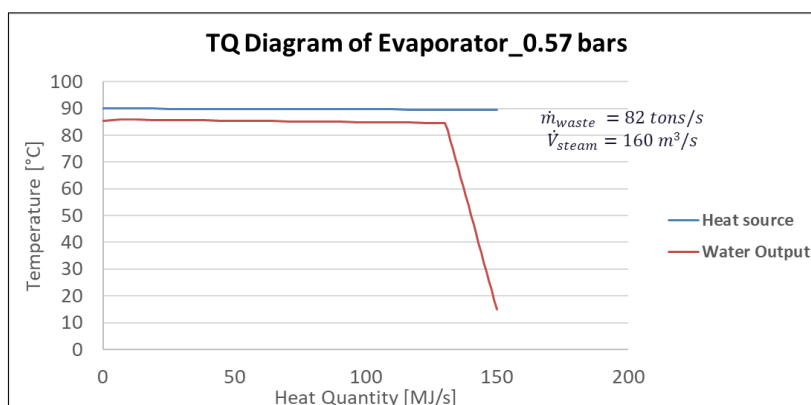


Figure 6.2.3. $T-\dot{Q}$ diagram of evaporator at the upper pressure limit

Figure 6.2.3 depicts the $T-\dot{Q}$ diagram of the steam evaporator at an evaporation pressure at 0.57 bars, which was the upper limit. The waste heat temperature at the inlet was fixed

to 90°C and the temperature of the feedwater inlet was 15°C, which was the assumed temperature if the feedwater was supplied from nearby sources (e.g rivers, lakes). As mentioned, the wastewater needs to be cooled down to at least 40°C so that it could be used in other cooling processes. At an evaporation pressure of 0.57 bars, water vaporizes at around 85°C, thus the temperature difference between the two fluids was very small. However, this prevented the wastewater from reducing its temperature to the required level. From the diagram, it shows that the slope of the wastewater temperature curve is limited by the curve of feedwater. If the outlet temperature of wastewater was lower, the two curves would overlap, resulting in a reverse heat transfer process. Therefore, the evaporation temperature of feedwater had to be reduced by lowering its pressure of vaporization to allow for the cooling of wastewater. Additionally, the required amount of waste heat increased greatly at higher steam evaporation pressure and became impossible to achieved at the rate of 82 tons/s at the upper limit.

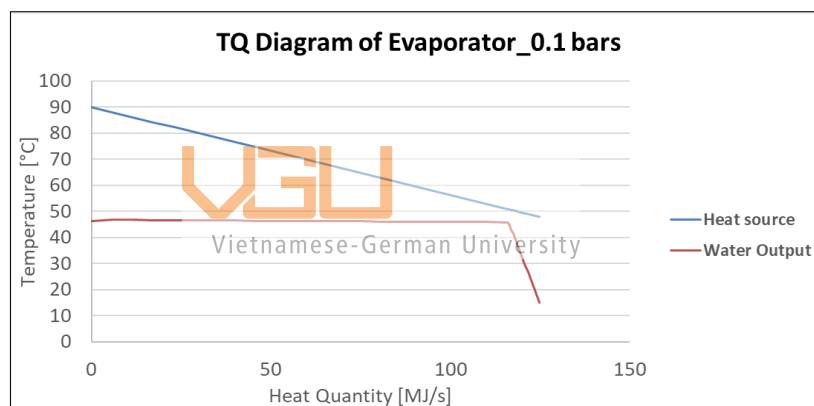


Figure 6.2.4. $T-\dot{Q}$ diagram of evaporator at the lower pressure limit

At the lower limit of 0.1 bars, the evaporation process happened at more than 45°C as demonstrated in figure 6.2.4. Although the temperature distribution of wastewater decreased drastically compared to the upper limit case, the outlet temperature could not reach the required temperature of 40°C. Moreover, the volumetric flow of steam was 710 m³/s at the lower limit, which was more than four times of the same figure at the upper limit of only 160 m³/s. This significant rise might cause the geometric design of the system to be infeasible.

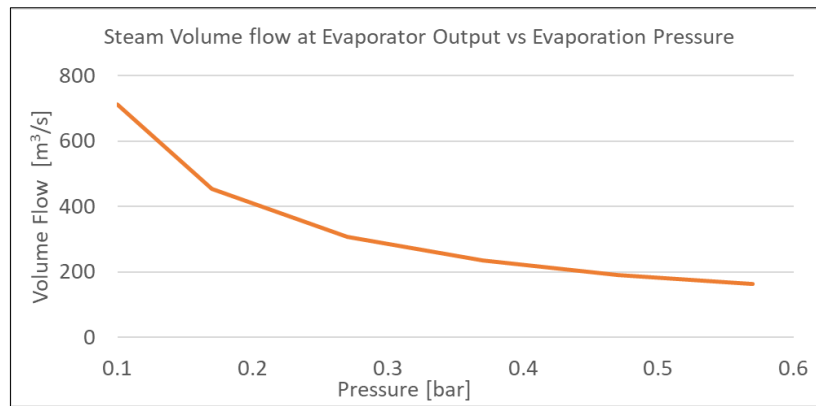


Figure 6.2.5. Volumetric flow of steam with respect to variation of steam evaporation pressure

As demonstrated in figure 6.2.5, the volumetric flow of steam at the evaporator outlet rose exponentially as the pressure was reduced. This result shows that the geometric design has to be taken into consideration in terms of feasibility. A greater volumetric flow meant the pipe diameter, or the velocity of the fluid had to increase. Either way, the limitation of the system geometry must be considered.

6.3. SHARC design Vietnamese-German University

6.3.1. Performance comparison

This section describes the performance of the two feasible variants of the SHARC system. In all variants, the steam extraction process took place in the Generation cycle. Regarding the assumptions, the charging time and discharging time were the same and the isentropic efficiency of all turbines was assumed to be 90%. On the other hand, the extracted power from the system was kept constant at 100 MW and the minimum pinch point in all heat exchangers was 2 K.

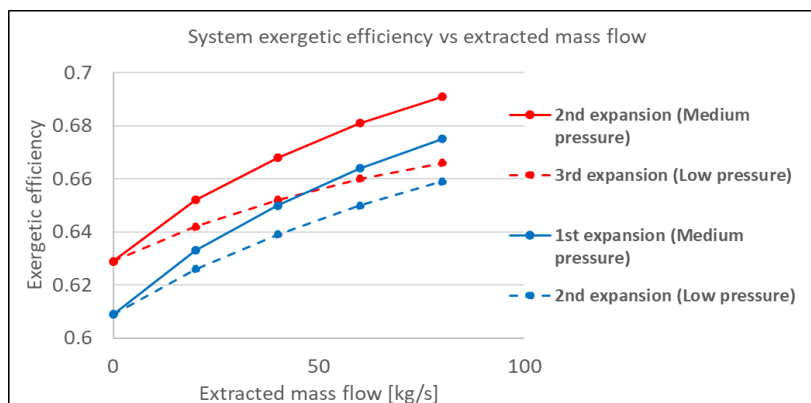


Figure 6.3.1. Summary diagram of SHARC's exergetic efficiency with respect to the variation of extracted steam mass flow

The first and foremost comparison was the exergetic efficiency analysis between the two systems, whose result is shown in figure 6.3.1. In the diagram, the curves with the same color (both dashed and solid) belong to the same system. The system that extracts steam from the second and third stages showed slightly better performance than the other. Hence, it was determined that this system would be used in further investigation.

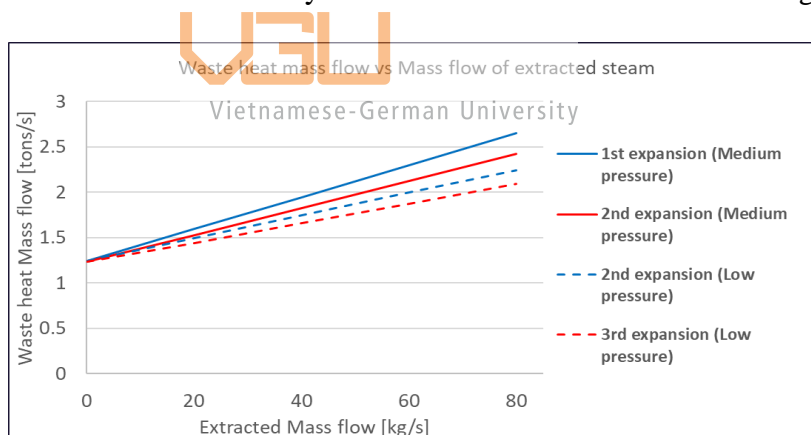


Figure 6.3.2. Summary diagram of required waste heat mass flow with respect to the variation of extracted steam mass flow

Figure 6.3.2. shows the mass flow of supplied wastewater for each case in terms of tons per second. The design that extracted steam from the endpoints of the second and third expansion stages also had the advantage of lower overall required amount of waste heat.

6.3.2. Maximum amount of extractable steam

Another essential aspect that had been analyzed was the highest mass flow of steam extraction that was possible for each system. This analysis only focused on the extraction of medium-pressure steam in the two variants of the SHARC design. The maximum amount of extractable steam for each variant is shown in figure 6.3.3.

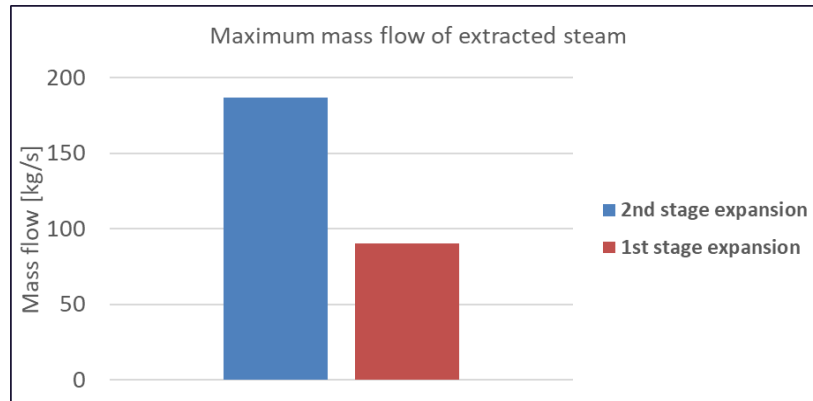


Figure 6.3.3. Maximum amount of extractable medium-pressure steam for each variant of SHARC module

For the system that extracted steam from the second expansion stage's endpoint, the limit was more than 180 kg/s. On the contrary, the maximum value for the system where steam was extracted from the first stage was recorded to be less than half of the previous variant, which was around 90 kg/s. A point to be noted here is that these maximal values would change with different amount of electricity generation power. However, the important point here is only the different amount between the two systems. It was shown that the factor limiting the amount of steam extraction was the temperature of the water outlet of the oil heat exchanger in the Charging cycle.

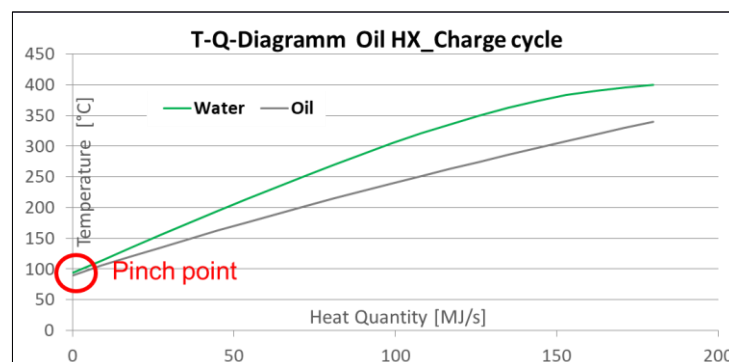


Figure 6.3.4. $T-\dot{Q}$ diagram of Oil heat exchanger in the Charging cycle

Further investigation of the system showed the reason for the limitation of steam extraction. Figure 6.3.4. illustrates the $T-\dot{Q}$ diagram for the Oil heat exchanger in the Charging cycle. The pinch point of this heat exchanger lay at the low-temperature terminal, where the outlet of water transferred heat to the inlet of the oil medium. As the amount of extracted steam increased, the lower the temperature of the water inlet became. The limit of the pinch point was 2 Kelvin, which meant that the water outlet temperature had to be at least 92°C since the lower boundary of the oil medium was 90°C . Due to the complexity of the SHARC design, the detailed analysis of how increasing the amount of steam extraction led to the reduction of this temperature was not conducted. Instead, it was determined that acknowledging the inversely proportional relation between the two parameters was sufficient.

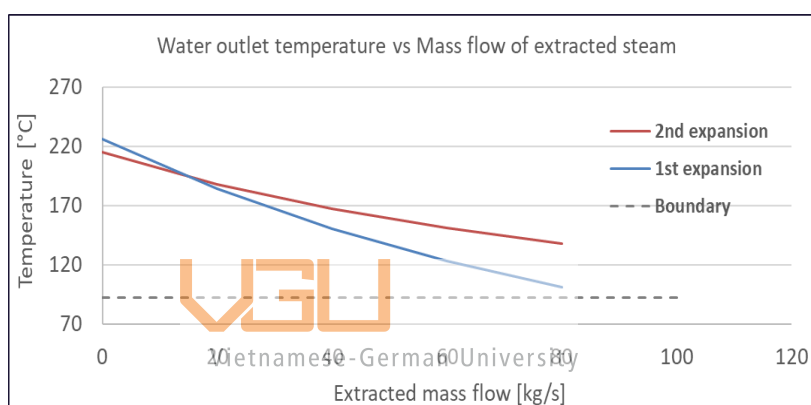


Figure 6.3.5. Outlet temperature of the water flow through Oil heat exchanger in the Charging cycle with respect to variation of extracted steam mass flow

The next step was to determine the reason for the difference in the amount of steam extraction between the two variants. Figure 6.3.5. depicts the rate of change of the water outlet temperature with respect to the increasing mass flow of steam extraction. The red curve shows the temperature of the outlet for the system that extracted medium-pressure steam from the endpoint of the second expansion stage, which has a smaller slope than the other system. This means that the red curve approaches the boundary line of 92°C slower than the blue curve in terms of increasing mass flow, meaning that the first expansion stage extraction system could only supply a smaller amount of steam compared to the other variant.

7. Final system

7.1. Overall architecture

Ultimately, the design of a complete system that satisfied all requirements of the chemical site was produced, whose schematic is exhibited in figure 7.1.1. The design combines two different systems that had been analyzed, including the industrial heat-pump design and the SHARC system.

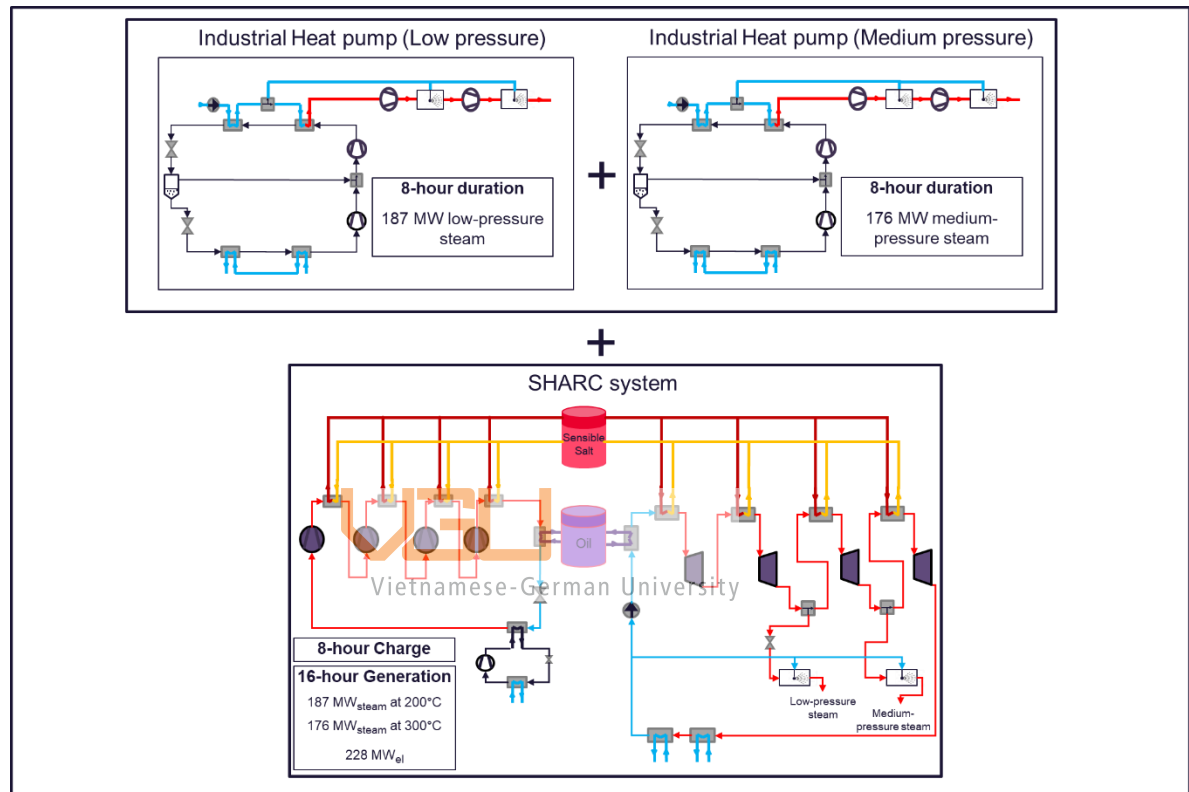


Figure 7.1.1. Schematic of the final design and requirements for each module

In summary, the complete system was required to run a total of 24-hour duration. During this time, low-pressure and medium-pressure steam must be generated at the rates of 187 MW and 176 MW respectively. Two separate industrial heat-pump systems were used for producing steam at different pressure levels, supplying for a total duration of 8 hours. Spray water was chosen to be the intercooling method for the heat pumps due to higher exergetic efficiency.

For the electricity generation requirement of 228 MW, the SHARC system which extracted steam from the endpoints of the second and third expansion stages was used to fulfil this demand. During the 24-hour duration, the first 8 hours are used for charging

the thermal storage whereas steam and electricity are generated in the remaining 16 hours. Power from the national electrical grid would be directly provided to the chemical sites during the Charging phase. Additionally, cold generation of 90 MW was a condition that needed to be achieved. However, this was not investigated and realized in the complete system.

7.2. CO₂ heat pump with Carnot battery system

Another system had already been investigated that had the same purposes of supplying steam and power to the chemical sites [Sul 22], which is illustrated in figure 7.2.1.

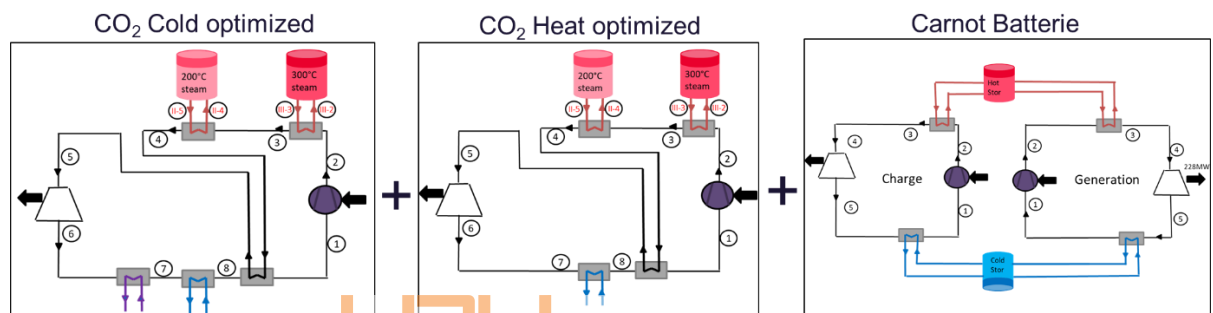


Figure 7.2.1. Schematic of the combined system of CO₂-based heat pump and Carnot battery
Vietnamese-German University

In general, the system consists of three modules that serve to produce steam and electricity. Two CO₂-based heat-pump cycles with preheating were used, in which one was optimized for cold generation while the other focused on heat generation. The third module worked on the principle of Carnot battery, which was similar to the SHARC design. Power is supplied to the system when the price is low, and electricity is generated while the cost of electricity rises. Additionally, this system had been designed to generate cold for storage by absorbing heat from the waste flow.

7.3. Performance comparison between two systems

Due to the lack of cold generation, an assumption had been made for the investigated system, which employed industrial heat pump and SHARC design, to be comparable. The system was assumed to have an artificial cold engine with a COP of 2.5, which represented the potential of the complete system with cold generation. Since the required

output of cold was 90 MW (for an 8-hour charge duration) at negative 20°C, the amount of power needed for this engine

would be 36 MW as deduced from the assumed value of COP. The exergy flow of the cold generation was calculated as exergy flow of heat

$$\dot{E} = \left(1 - \frac{T}{T_a}\right) \cdot \dot{Q}$$

In which T is the cold flow temperature, T_a is the ambient temperature and \dot{Q} is the amount of heat flow. The cold flow temperature T was 253.15 K (or -20°C) while ambient temperature T_a was 288.15 K (or 20°C). The value for the heat flow \dot{Q} was the output requirement of 90 MW. With the obtained values for the cold engine, calculations for the comparison could be performed.

For the comparison, the two systems were examined under the same set of boundary conditions listed in section 3, but with the wastewater inlet temperature of 34°C and outlet temperature of 20°C. The results of this analysis are shown in table 7.1. below.

Table 3. Power consumption and exergetic efficiency of the current and previous systems

Parameters	CO ₂ heat pump with Carnot battery (H ₂ O)	CO ₂ heat pump with Carnot battery (Air)	Industrial heat pump with SHARC	Industrial heat pump with SHARC (Corrected)
P_{in} [MW]	1324	1441	1249	1285
η_{ex} [%]	63	58.2	66.2	65.2

The amount of power supplied to the system and the system's exergetic efficiency were the two main parameters used for comparing the performance. The first two columns of table show the results for the previous system variants. The first column is for the variant that used water-based Carnot battery while the second one is for the variant that operated on air. For the industrial heat pump with SHARC design that did not consider the cold engine, the results are displayed in the third column. The fourth column presents data for the same system but with consideration of the cold engine (corrected).

Overall, the calculations show that the combined system of industrial heat pump and SHARC design (both with and without cold engine) produced a higher exergetic efficiency and slightly lower power consumption compared. Specifically, an exergetic efficiency difference of 2.2% -points and 40 MW lower input power could be seen for the “corrected” design of industrial heat pump and SHARC compared to the system of CO₂ heat pump with Carnot battery operating on water. Therefore, the investigated system had an advantage in terms of thermodynamic performance over the previous system.



Vietnamese-German University

8. Conclusion

The purpose of this paper is the thermodynamic design and evaluation of a system that generates steam and power for chemical sites. Based on the performance analyses of different concepts of high-temperature heat pump, a final design for this system had been produced, which consisted of two industrial heat pump modules and the SHARC module. Then, this system was compared to a previous design of CO₂-based heat pump with Carnot battery, showing slightly better performance.

The constraint variation analysis for the industrial heat pump was conducted first, in which the steam evaporation pressure and the temperature of waste heat at the inlet and outlet were varied. Results showed that at lower pressure of evaporation in the range of 0.45 to 0.65 bars, the system could reach optimal performance. However, the volumetric flow of steam increased exponentially at lower evaporation pressure, leading to greater demand on the system geometric design. On the other hand, higher inlet and outlet temperature of waste heat led to greater exergetic efficiency and COP. The increment of the outlet temperature had greater effect on the system behavior but at the cost of higher required wastewater mass flow.

For the SHARC module, a similar variation analysis was conducted, in which the amount of extracted steam and temperature of the waste heat were adjusted. The exergetic efficiency of the system became higher as the amount of steam extraction increased. The wastewater and system mass flows in the Charging, Generation and heat-pump cycles had to increase to supply the increasing steam amount. Conversely, the waste heat temperature variation also produced similar pattern to the industrial heat pump system. The system exergetic efficiency was greater at higher inlet and outlet temperature of the wastewater, with the cost of higher required mass flow at higher outlet temperature.

Different variants of the system modules were created and compared. For the industrial heat pump, there were two mechanisms of intercooling that had been examined, which were by spray water and heat storage. The conclusion of the comparison at baseline conditions was that the system that used spray water saw around 3% higher COP and exergetic efficiency than the heat storage method. It was deduced that the poorer performance from the usage of heat storage was due to the losses incurred by the inclusion of additional heat exchangers. Therefore, spray water was chosen as the intercooling method for industrial heat pump design.

The special variant with direct evaporation without the use of heat pump created specifically for the case of 90°C waste heat inlet temperature reported great performance. The system's COP of up to 3.5 and exergetic efficiency of nearly 1.2 (if the exergy of wastewater was not considered) could be reached at the upper limit of steam evaporation pressure. However, one major problem of this system was that the requirement of cooling wastewater down to at least 40°C was not possible. Other drawbacks included significant required amount of waste heat at the upper limit and volumetric flow of steam at lower limit. Thus, this design was not considered further.

Two variants were created for the SHARC design. The first variant extracted medium- and low- pressure steam from the endpoints of the second and third expansion stages of the Generation cycle, whereas the second variant extracted steam from the first and second expansion stages. Overall, the comparison reported that the first variant had greater exergetic efficiency of roughly 1% to 2%-points. Moreover, the first variant also showed the potential for higher rate of extractable steam mass flow compared to the second variant. As a result, the first variant, in which steam after the second and third expansion stages was extracted, was selected for the final design.

Finally, the complete design was created, including two separate industrial heat pumps working in parallel and the SHARC system. Comparison with a previous design of CO₂ heat pump with the water-based Carnot battery showed that the combination of industrial heat pumps and SHARC module provided better performance. Specifically, the combined system of industrial heat pumps and SHARC saw an exergetic efficiency improvement of 2.2%-points and around 40 MW lower power consumption when operating under the same boundary and output conditions. Hence, it was concluded that this system was thermodynamically more efficient and showed good potential for industrial applications. However, other aspects of the system must be examined before deciding which design was the most optimal, such as the geometric design, availability of the components and so forth.


9. Outlook


The complete system demonstrated satisfactory performance at baseline conditions. However, this system can still be thermodynamically fine-tuned to bring out better performance. Therefore, the next logical step would be to optimize the design. The geometric design and cost analysis of the final system should also be performed to examine the feasibility and practicability of the system compared to previously investigated design. Then, different load cases of the system can be computed and analyzed. For example, the required conditions to perform a cold start of the system is essential to be determined. Additionally, load cases where the output requirements are different from the given reference paper should also be calculated since the demands from the chemical sites are not always constant.

Another approach can be taken for the redesign of the complete system. Instead of using industrial heat pumps to generate steam during the Charging phase, steam can be extracted directly from the Charging cycle of the SHARC module or by using stored thermal energy to generate. This will eliminate the usage of additional heat pump design. Then, similar analyses of constraint variation and performance comparison can be performed.



Bibliography

- [ABU+ 18] Arpagaus, C.; Bless, F.; Uhlmann, M.; Schiffmann, J.; Bertsch, S. (2018): *High temperature heat pumps: Market overview, state of the art, research status, refrigerants, and application potentials*. In: Energy, Vol. 152, pp. 985-1010.
- [ACC+ 16] Aga, V.; Conte, E.; Carroni, R., Burcker, B.; Ramond, M. (2016): *Supercritical CO₂-Based Heat Pump Cycle for Electrical Energy Storage for Utility Scale Dispatchable Renewable Energy Power Plants*. 5th International Symposium – Supercritical CO₂ Power Cycles, San Antonio, Texas.
- [BPK+ 22] Bauer, T.; Prenzel, M.; Klasing, F.; Franck, R.; Lützow, J.; Perrey, K.; Faatz, R.; Trautmann, J.; Reimer, A.; Kirschbaum, S. (2022): *Ideal-Typical Utility Infrastructure at Chemical Sites – Definition, Operation and Defossilization*. In: Chemie Ingenieur Technik, Vol. 94 , No. 6, pp. 840-851.
- 
Vietnamese-German University
- [Bro 05] Brown, R. N. (2005): *Compressors: Selection and Sizing. 3rd edition*, Elsevier.
- [Cas 22] Compressed Air and Fluid Solutions USA (CASCOUSA) : *Single and Multiple Stage Compressors*. <https://cascousa.com/compressed-air-101/types-of-compressors/single-versus-multi-stage-compressors/>. Accessed on November 17th , 2022.
- [CAN 22] Climate Action Network Europe: *CAN Europe's transformation pathway recommendations for the chemical industry*. <https://caneurope.org/can-europes-transformation-pathway-recommendations-for-the-chemical-industry>. January 28th, 2022.
- [CCY 10] Chua, K. J.; Chou, S. K.; Yang, W. M. (2010): *Advances in heat pump systems: A review*. In: Applied Energy, Vol. 87, No. 12, pp. 3611-3624.

- [CeBo 15] Çengel, Y. A.; Boles, M. A. (2015): *Thermodynamics: An Engineering Approach*. 8th edition, McGrawHill, New York, United States of America.
- [CPE 12] Cole, W.; Powell, K.; Edgar, T. (2012): *Optimization and advanced control of thermal energy storage systems*. In: *Reviews in Chemical Engineering*.
- [DiRo 20] Dincer, I.; Rosen, M. A. (2020): *Exergy. Energy, Environment and Sustainable Development*. 3rd edition.
- [Gra 18] Grassi, W. (2018): *Heat pumps. Fundamentals and Applications*. 1st edition. Springer Cham.
- [Hor 14] Horbaniuc, B. D. (2014): *Refrigeration and air-conditioning*. In: *Encyclopedia of Energy*, Vol. 5.
- [HuAn 10] Huleihil, M.; Andresen, B. (2010): *Generalized Performance Characteristics of Refrigeration and Heat Pump Systems*. In: *Physics Research International*.

Vietnamese-German University
- [HZB+ 16] Huang, F.; Zheng, J.; Baleynaud, J. M.; Lu, J. (2016): *Heat recovery potentials and technologies in industrial zones*. In: *Journal of the Energy Institute*, Vol. 90, No. 6, pp. 951-961.
- [Kir 15] Kirova-Yordanova, Z. (2022): *Low Temperature Waste Heat in Chemical Industry: Problems and Possible Ways to Recover the Heat of Condensation*. The 28th International Conference on Efficiency, Cost, Optimization, Simulation and Environmental Impact of Energy Systems, France.
- [KRD+ 16] Kumar, Y.; Ringenberg, J.; Depuru, S. S.; Devabhaktuni, V. K.; Jin, W. L.; Nikolaidis, E.; Andersen, B.; Afjeh, A. (2016): *Wind energy: Trends and enabling technologies*. In: *Renewable and Sustainable Energy Reviews*, Vol. 53, pp. 209-224.

- [KSM 20] Krtková, E.; Saarikivi, R.; Müllerová, M. (2019): *Approximated EU greenhouse gas inventory. Proxy GHG emission estimates for 2019*. Report for the European Topic Centre on Climate change mitigation and energy (ETC/CME)
- [McG 14] McGovern, J. (2014): *Applied Energy Systems – Rudimentary Thermodynamics*.
- [MSS 11] Mekhilef, S.; Saidur, R.; Safari, A. (2011): *A review on solar energy use in industries*. In: *Renewable and Sustainable Energy Reviews*, Vol. 15, No. 4, pp. 1777-1790.
- [MSZ+ 21] Marina, A.; Spoelstra, S.; Zondag, H.; Wemmers, A. (2021): *An estimation of the European industrial heat pump market potential*. In: *Renewable and Sustainable Energy Reviews*, Vol. 139, 110545.
- [NLN 19] Nwakpang, I.; Lebele-Alawa, T.; Nkoi, B. (2019): *Performance Assessment of A Two-Stage Reciprocating Air Compressor*. In: *European Journal of Engineering Research and Science*, Vol. 4, No.4, pp. 74-82. Vietnamese-German University
- [PGZ 17] Pezzutto, S.; Grilli, G.; Zambotti, S. (2017): *European Heat Pump Market Analysis: Assessment of Barriers and Drivers*. In: *International Journal of Contemporary ENERGY*, Vol. 3, No. 2.
- [Sul 22] Sulberg, C. (2022): *Konzeptentwicklung einer Hochtemperaturwärmepumpe für einen Industriestandort auf Basis zeotroper Gemische*. Master Thesis.
- [Sie 22] Siemens Energy (2022): *CO2 neutrale Energieversorgung von Industriestandorten am beispiel eines Chemieparks*. Status meeting.
- [ZBB+ 19] Zühlsdorf, B.; Bühler, F.; Bantle, M.; Elmegaard, B. (2019): *Analysis of technologies and potentials for heat pump-based process heat supply above 150°C*. In: *Energy Conversion and Management: X*, Vol. 2, 100011.

- [ZHX+ 14] Zhu, N.; Hu, P.; Xu, L., Jiang, Z., Lei, F. (2014): *Recent research and applications of ground source heat pump integrated with thermal energy storage systems: A review*. In: Applied Thermal Engineering, Vol. 71, No.1, pp. 142-151.
- [WaZh 18] Wang, R.; Zhai, X. (2018): *Handbook of Energy Systems in Green Buildings*. 1st edition. Springer Berlin, Heidelberg.



Vietnamese-German University



Vietnamese-German University

RUHR-UNIVERSITÄT BOCHUM

Fakultät für Maschinenbau
Lehrstuhl für Thermodynamik